Biomaterials 329 (2026) 123985

Contents lists available at ScienceDirect

Biomaterials

journal homepage: www.elsevier.com/locate/biomaterials

An antioxidant, injectable hydrogel with mitochondrial fusion effect promotes inflamed dental pulp repair via immunomodulation and reactive oxygen species scavenging

Dan Wang [a,1], Yongle Lv [b,1], Fei Xie [a], Yanqiang Zhao [a], Bowen Ren [a], Shanshan Jin [a], Ningxin Zhu [a], Man Qin [a], Zhiqiang Lin [c], Lei Wang [b,*], Yuanyuan Wang [a,**]

[a] Department of Pediatric Dentistry, Peking University, School and Hospital of Stomatology, #22 Zhongguancun Nandajie, Haidian District, Beijing, 100081, China
[b] Beijing Advanced Innovation Center for Materials Genome Engineering, State Key Laboratory for Advanced Metals and Materials, School of Materials Science and Engineering, University of Science and Technology Beijing, #30 Xueyuan Road, Haidian District, Beijing, 100083, China
[c] Institute of Systems Biomedicine, Beijing Key Laboratory of Tumor Systems Biology, School of Basic Medical Sciences, Peking University Health Science Center, Beijing, 100191, China

ARTICLE INFO

Keywords:
Macrophage polarization
Mitochondrial fusion
Metabolic-flux analysis
Chitosan hydrogel
Antioxidation
Immunoregulation

ABSTRACT

Vital dental pulp is crucial for the self-repair and long-term retention of teeth with pulpitis; pulp capping materials used for vital pulp therapy must involve controlling inflammatory cascade and regulating inflammatory microenvironment at the same time. Here, we designed a dual-effect hydrogel with immunoregulatory and antioxidant properties to achieve inflamed pulp tissue repair. MASM7, a "mitochondrial glue" promoting mitochondrial fusion, could modulate THP-1-derived macrophages (THP-1-M) polarization to the M2 type under LPS-stimulated inflammatory conditions. Seahorse assay and metabolic-flux analysis (MFA) revealed that mitochondrial fusion modulated metabolic reprogramming of THP-1-M under inflammation from glycolysis to OXPHOS. Moreover, MASM7-treated THP-1-M cells enhanced the repair ability of DPSCs under inflammatory conditions. To realize the application of MASM7 and antioxidant property, chitosan (CS) and methacrylic anhydride (MA) were used to synthesize a methacrylated CS (CSMA) hydrogel, which was then modified with gallic acid (GA) to form a CSMAGA hydrogel. We next confirmed the biocompatibility of this hydrogel. The CSMAGA hydrogel also demonstrated antioxidant properties by scavenging reactive oxygen species. We then confirmed the dual effects of MASM7@CSMAGA hydrogel in rats with LPS-stimulated pulpitis. In conclusion, MASM7@CSMAGA hydrogel can promote pulp tissue repair under inflammatory conditions by modulating macrophage polarization and oxidative stress.

1. Introduction

Pulpitis, a common dental disease, is conventionally treated with root canal therapy, which involves the complete removal of vital dental pulp. However, it causes the tooth to enter a non-physiological state; this is detrimental to the ongoing development of young permanent teeth and long-term retention of mature permanent teeth, potentially warranting considerably complicated and expensive treatments in the future. Nevertheless, recent studies have suggested that the pulp tissue somewhat retains its self-repair capacity during pulpitis [1]. Vital pulp therapy (VPT) can be used to treat pulpitis, avoids the complete removal of pulp tissue by applying biologic pulp capping materials. The biological performance of pulp capping materials is a key factor influencing the success rate of VPT. An ideal pulp capping material should possess immunomodulatory capacity and be able to reshape the inflammatory microenvironment of the dental pulp tissue. However, current pulp

* Corresponding author. School of Materials Science and Engineering, University of Science and Technology Beijing, #30 Xueyuan Road, Haidian District, Beijing, 100083, China.
** Corresponding author.
E-mail addresses: elsie_0617@foxmail.com (D. Wang), lvyongle202210341@163.com (Y. Lv), fei.xie@pku.edu.cn (F. Xie), 2211210555@stu.pku.edu.cn (Y. Zhao), 1910303106@pku.edu.cn (B. Ren), jinss1022@163.com (S. Jin), momouniverse2625@163.com (N. Zhu), qin-man@foxmail.com (M. Qin), Zhigiang_lin@bjmu.edu.cn (Z. Lin), lei_wang@ustb.edu.cn (L. Wang), cwyyd@126.com (Y. Wang).
[1] These authors contributed equally to this work.

https://doi.org/10.1016/j.biomaterials.2026.123985
Received 9 September 2025; Received in revised form 14 December 2025; Accepted 3 January 2026
Available online 4 January 2026

capping materials such as calcium silicate cements (CSCs) and mineral trioxide aggregate (MTA) are facing several clinical challenges in the inflammatory microenvironment, including persistent chronic inflammation and "ectopic calcification" of residual pulp tissue. A novel pulp capping material is needed by controlling the inflammatory cascade, regulating the pulp tissue inflammatory microenvironment, and promoting pulp tissue self-repair. Recent studies have also reported a range of pulp capping materials with immunomodulatory capacity or inflammatory microenvironment reshaping ability respectively. Thus, a biological pulp capping material with both effects is in urgent need of design.

The immune microenvironment has a pivotal regulatory role in inflammatory tissue repair. Macrophages, the primary immune cells within the human body, undergo alterations during the bacterial elimination, wound-healing, and tissue regeneration processes [2–4]. The inflammatory response within the dental pulp tissue is relatively mild [5], where M1 macrophages eliminate bacteria and remove necrotic cells, and M2 macrophages secrete anti-inflammatory cytokines and elicit tissue repair-promoting signals [6,7]. However, as an infection aggravates, macrophage polarization toward the M1 type escalates, whereas that toward the M2 type is impeded; this consequently results in the inhibition of inflammatory dental pulp tissue repair and regeneration [8]. Moreover, a major challenge impedes inflamed pulp tissue repair: under inflammatory conditions, macrophages cannot efficiently polarize to the anti-inflammatory and pro-repair M2 type.

Mitochondria, the powerhouse of a cell, have garnered considerable attention recently because they are strongly associated with the modulation of macrophage polarization [9,10]. Mitochondrial function is a prerequisite for M2 macrophage induction under inflammatory conditions [11]. Mitochondrial dynamics, including processes underlying morphological remodeling, encompasses mitochondrial morphology reshaping via fission and fusion processes regulated by proteins related to fission (e.g., DRP-1, FIS, and MFF) and fusion (e.g., MFN1 and MFN2), respectively [12,13]. In particular, mitochondrial fission is intricately linked to macrophage polarization toward M1 type, which harbor fragmented mitochondria and predominantly depend on glycolysis for their metabolic needs. In contrast, mitochondrial fusion is pivotal in the M2 polarization of macrophages. During this process, macrophages have elongated mitochondria, which enable increased oxidative phosphorylation, that facilitates M2 polarization [14–16]. The fusion of the outer mitochondrial membrane, a pivotal initial phase in the mitochondrial fusion process, is regulated by mitochondrial fusion-associated proteins, namely MFN1 and MFN2, and includes three sequential steps: tethering, docking, and merging [17]. In primates, MFN2 exhibits membrane tethering efficiency superior to MFN1 [18]. Consequently, MFN2 targeting may enhance mitochondrial fusion more efficiently. Modulating the conversion of MFN2 from its anti-tethering conformation to its pro-tethering conformation is a crucial strategy facilitating mitochondrial fusion [19]. MASM7, a novel mitochondrial fusion activator, is a small-molecule compound derived from pharmacophore simulation through in silico screening [20]. MASM7 mimics the helical peptide 367–384Gly in residues from the MFN2 HR-1 domain, which is vital in determining pro-tethering conformation conversion [21]. This compound demonstrates a "mitochondrial glue" effect: It competitively binds to the HR-2 domain of MFN2 and disrupts the HR1–HR2 domain interaction, which results in the release of the HR-1 domain and then prompts the transition of MFN2 into its pro-tethering conformation; consequently, mitochondrial fusion occurs. As such, we propose using MASM7 to promote macrophage mitochondrial fusion and thereby modulate the immune microenvironment of inflamed dental pulp.

In dental pulp, the inflammatory microenvironment can cause resident cells to undergo oxidative stress, which is another crucial factor impeding inflamed dental pulp repair [22,23]. In particular, excessive reactive oxygen species (ROS) production within this inflammatory milieu can induce oxidative stress and disrupt redox homeostasis, culminating in oxidative damage to critical biomolecules, such as lipids, DNA, and proteins [24,25]. Oxidative stress has been implicated in the development of many diseases (e.g., cardiovascular and neurodegenerative diseases and diabetes), as well as in aging; it also plays a role in hindering tissue healing [26–28]. As previously reported, during pulpitis, anti-oxidative stress materials can bolster the reparative potential of mesenchymal stem cells in pulp tissue, facilitating their differentiation into odontoblasts and thereby fostering inflamed dental pulp tissue repair [29]. Thus, mitigating oxidative stress by neutralizing excess ROS may be a highly effective strategy for inflamed dental pulp tissue repair.

Chitosan (CS) hydrogels, derived from the natural polysaccharide CS, have been applied across various domains, including hemostasis [30], wound healing [31], and scaffolds in tissue engineering [32]; they have also been used in the repair of inflamed dental pulp [33]. Recently, CS hydrogels have been modified with methacrylic anhydride (MA) to obtain methacrylated CS (CSMA) hydrogels, which have photo-cross-link capabilities, making them suitable for drug and protein delivery [34,35]. CSMA hydrogels have several desirable properties, such as rapid gelation in situ and improved injectability. These features collectively allow these hydrogels to fit the irregular morphology of inflamed dental pulp tissue, thus enabling targeted local application and drug delivery. However, CSMA hydrogels have limited antioxidant properties. Modifying CSMA hydrogels with antioxidant compounds may considerably improve their pro-repair effects in inflamed pulp tissue. Gallic acid (GA), a natural compound from plants featuring a pyrogallol-like structure, may impart antioxidant capabilities to CSMA hydrogels [36]. Pyrogallol is a phenolic group with a notable benzene-1, 2,3-triol structure, which imparts compounds with free radical scavenging activity [37], allowing them to substantially alleviate oxidative stress.

In the current study, we first validated whether MASM7, as a mitochondrial glue, facilitates macrophage polarization toward the M2 type by mediating mitochondrial from over-fission to fusion under inflammatory conditions. We further confirmed its immunomodulatory effects in inflamed dental pulp stem cells and explored the underlying mechanisms. Subsequently, we modified CSMA hydrogels with GA to synthesize a photo-cross-linkable, injectable hydrogel with anti-oxidative stress effects and deliver MASM7 to achieve immunomodulatory effects. Finally, to verify the dual effects of the hydrogel in vivo, we established a pulpitis rat model and applied the hydrogel locally.

2. Materials and methods

2.1. Cell culture

THP-1 monocytes from company (Procell, Wuhan, China) were cultured in RPMI 1640 medium supplemented with 10 % fetal bovine serum (FBS), 1 % penicillin-streptomycin, and L-glutamine. We then induced the differentiation of THP-1 monocytes to THP-1 macrophage-like (THP-1-M) cells by culturing THP-1 monocytes with 80 ng/mL phorbol 12-myristate 13-acetate (PMA) for 12 h. Finally, adherent cells (i.e., THP-1-M cells) were washed, cultured in PMA-free medium, and used for further experimentation.

Human dental pulp stem cells (hDPSCs) were kindly provided by Oral Stem Cell Bank operated by Beijing Tason Biotech Co. Ltd. (http://www.kqgxb.com). These hDPSCs were cultured in minimum essential medium α (α-MEM) supplemented with 10 % FBS and 1 % penicillin-streptomycin. Passage 4–6 hDPSCs were used for the subsequent experiments.

Commercially available human Peripheral Blood Mononuclear Cells (hPBMC) induced M0 macrophages(hPBMDM) from company (Milecell Bio, Shanghai, China) were cultured in RPMI 1640 medium supplemented with 10 % fetal bovine serum (FBS), 1 % penicillin-streptomycin and used for further experimentation.

2.2. Mitochondrial morphology analysis

THP-1-M cells were cultured in confocal dishes, exposed to 500 ng/mL lipopolysaccharide (LPS) for 12 h, and either treated or not treated with 1 μg/L MASM7. Next, mitochondrial staining was performed using PK mito and detected through super-resolution optical microscopy. The average perimeter, average area, mean branch length, and aspect ratio of the mitochondria were calculated using MiNA 2.0 [38]. Moreover, transmission electron microscopy (TEM) was also used to observe mitochondrial morphology.

2.3. Quantitative polymerase chain reaction

Total RNA was extracted using TRIzol reagent (Invitrogen, USA), and 500 ng of total RNA was converted to complementary DNA by using a PrimeScript RT Reagent Kit (Takara, Japan). Next, quantitative polymerase chain reaction (qPCR) was performed in triplicate, as described previously [39]. Table S1 lists all primers used here.

2.4. Enzyme-linked immunosorbent assay

THP-1-M cells were treated with LPS and MSAM7. The supernatants were harvested and kept at −80 °C until use. The levels of the inflammatory factors tumor necrosis factor (TNF) α, interleukin (IL) 1β, and IL-6 in the supernatants were measured using a commercial enzyme-linked immunosorbent assay kit (Liankebio, Hangzhou, China) and a luminometer plate reader (Molecular Devices, CA), according to the manufacturer's instructions.

2.5. Immunofluorescence staining

THP-1-M cells were exposed to 500 ng/mL LPS for 12 h and then treated or not treated with 1 μM MASM7. Thereafter, they were fixed in 4 % paraformaldehyde for 10 min, permeabilized with 0.1 % Triton X-100 for 5 min, and blocked with 5 % bovine serum albumin for 2 h. Next, the fixed cells were incubated with the following primary antibodies from (Proteintech) USA at 4 °C overnight: anti-CD68 (66231-2-lg), anti-CD86 (13395-1-AP), anti-CD206 antibody (18704-1-AP). Subsequently, they were incubated with secondary antibodies (Proteintech, USA) at 37 °C for 1 h. Moreover, 4′,6-diamidino-2-phenylindole (DAPI; Solibro, China). Images were captured with the confocal imaging system Olympus FV3000 (Olympus, Japan).

2.6. Seahorse assay

We measured the oxygen consumption rate (OCR) and extracellular acidification rate (ECAR) of the THP-1-M cells on the Seahorse XFe96 analyzer (Agilent, USA) by using a Cell Mito Stress Test Kit (103015-100; Agilent, USA) and Glycolytic Rate Assay Kit (103344-100; Agilent, USA), respectively, according to the manufacturer's instructions. In brief, THP-1 cells were seeded in 96-well Seahorse assay plates at 1.5×10^5 cells per well and induced to transform into THP-1-M cells. After the attachment, the cells were exposed to 500 ng/mL LPS for 12 h and then treated or not treated with 1 μM MASM7. The cells were then washed, and the culture medium was replaced with Seahorse XF RPMI supplemented with 20 mM glucose, 2 mM L-glutamine, and 1 mM sodium pyruvate. To determine the OCR, 1.5 μM oligomycin, 1.5 μM FCCP, and 0.5 μM rotenone/antimycin A (Rot/AA) were added sequentially, and oxygen consumption contribution and sources were evaluated. To measure the ECAR, Rot/AA was added at 0.5 μM and 2-DG was added at 50 mM sequentially.

2.7. Targeted metabolomics

THP-1-M cells were induced as indicated in Section 2.6. The cells were then washed with phosphate-buffered saline (PBS) and rapidly frozen in liquid nitrogen for metabolic extraction. The cells were then sent to Novogene (Beijing, China) for targeted metabolomic analysis based on liquid chromatography (LC)–mass spectrometry (MS) of glycolysis and the tricarboxylic acid (TCA) cycle.

2.8. Metabolic flux analysis (MFA)

100 % labeled ^{13}C-D-glucose were added to RPMI 1640 medium without glucose(at a concentration 2 g/L). THP-1-M cells were induced as indicated in Section 2.6. The cells were then washed with PBS and cultured in the labeled medium for 6 h. After that, cells were collected on dry ice to 1 mL cold 50 % methanol. MFA were performed by Shanghai Biotree Biotech Co.,Ltd. using GC-MS analysis and followed a previously published protocol [40]. Then, GC/MS data were analyzed to determine isotope labeling and quantities of metabolites. To determine ^{13}C labeling, the mass distribution for known fragments of metabolites was extracted from the appropriate chromatographic peak. For each fragment, the retrieved data comprised mass intensities for the lightest isotopomer (without any heavy isotopes, M0), and isotopomers with increasing unit mass (up to M6) relative to M0. These mass distributions were normalized by dividing by the sum of M0 to M6 and corrected for the natural abundance of heavy isotopes of the elements H, N, O, Si and C, using matrix-based probabilistic methods as described [41], and implemented in code.

2.9. Cell coculture

DPSCs and THP-1-M cells were seeded in the lower and upper compartments of 12-well transwell plates (0.4 μm) for coculture, respectively. THP-1-M cells were exposed to 500 ng/mL LPS for 12 h and then treated or not treated with 1 μM MASM7. Odontogenic differentiation was induced in DPSCs through exposure to osteogenic medium (OM) for 14 days. Odontogenic differentiation markers of the cocultured DPSCs were detected through ALP staining, ARS staining, and qPCR. After coculture, total RNA in the DPSCs was extracted using TRIzol reagent and subjected to RNA sequencing.

For hPBMDM and DPSCs co-culture, hPBMDM were seeded in the upper compartments of 12-well transwell plates. Odontogenic differentiation was induced in DPSCs through exposure to osteogenic medium (OM) for 10 days. Other protocols were same as THP-1-M.

2.10. ALP and ARS staining

ALP staining was performed on day 7 of coculture by using an ALP staining kit (CWbio, Beijing, China), according to the manufacturer's protocol. In brief, DPSCs in the lower compartment were rinsed with PBS and fixed with 4 % paraformaldehyde. Then, they were incubated in an alkaline solution at room temperature for 10 min.

For ARS staining, the DPSCs were stained with 0.1 % ARS (pH 4.0–4.6) for 20 min. Finally, the reaction was terminated with clean water.

2.11. Western blotting

On day 14, DPSCs were harvested using a protein lysis buffer containing a phosphatase inhibitor (Applygen Technologies, Beijing, China), followed by centrifugation at 12,000 g at 4 °C for 30 min. Protein concentrations in the lysates were determined using a BCA assay kit (CWBIO, Beijing, China). Then, the lysates were loaded at equal amounts (20 μg) of total protein in each lane of a polyacrylamide gel and subjected to sodium dodecyl sulfate polyacrylamide gel electrophoresis. Next, they were transferred onto polyvinylidene difluoride membranes (Millipore, Bedford, MA), blocked with 5 % bovine serum albumin for 2 h, and probed with antibodies against the autophagy marker DSPP (1:1000; Santa Cruz, USA) and β-actin (1:10,000; Cell Signaling Technology, Beverly, MA, USA) at 4 °C overnight. Next, they were incubated

with horseradish peroxidase-conjugated antirabbit immunoglobulin at room temperature for 1 h, and protein expression was detected using a chemiluminescence blotting kit (Solibro, Beijing, China).

2.12. RNA sequencing

DPSCs were cocultured with THP-1-M cells for 3 days as described in Section 2.8. Total mRNA was extracted from DPSCs in the treatment groups and subjected to transcriptome sequencing at Tsingke (Beijing, China).

2.13. CSMA and CSMAGA synthesis

CS (viscosity >400 mPa s, degree of deacetylation = 83.5 %), MA (98 %), lysozyme (from egg white; ≥30,000 FIP-U/mg cryst), and GA (97.5 %) were acquired from Shanghai Sigma-Aldrich Trading. Moreover, we procured N-(3-dimethylaminopropyl)-N′-ethylcarbodiimide hydrochloride (EDC·HCl, 98 %) from Shanghai Aladdin Biochemical Technology, glacial acetic acid from Shanghai MacLean Biochemical Technology, lithium salt of phenyl-2,4,6-trimethylbenzoylphosphonic acid (LAP; 99 %) from Huaxia Siyin Biotechnology, and ethanol (99 %) from Modern Oriental (Beijing) Technology Development.

CS powder (1 g) was completely dissolved in a 1 % v/v acetic acid solution (100 mL) at 25 °C. We then added MA solution (1.41 mL) with continuous stirring at 60 °C in the dark for 6 h. Next, the pH of this mixture was adjusted to 7.0 using saturated $NaHCO_3$. The resulting solution was dialyzed against deionized water for 3 days to remove unreacted MA and byproducts. Finally, we freeze-dried the dialyzed solution to obtain CSMA. The degree of substitution (DS) was calculated as follows:

$$DS = \frac{I_{5.45\text{-}5.85}/2}{I_{1.74\text{-}1.83}/3} \times 16.5\% \quad (1)$$

where $I_{(5.45–5.85)}$ and $I_{(1.74–1.83)}$ denote the integrated areas of the methylene protons (carbon–carbon double bond) peak at 5.45–5.85 ppm and the methyl proton peak at 1.74–1.83 ppm, respectively.

For CSMAGA synthesis, CSMA sponge (0.25 g) was completely dissolved in deionized water (25 mL) at 25 °C, and GA (0.249 g) was completely dissolved in ethanol (2.5 mL). EDC, a coupling reagent (0.280 g, molar ratio of EDC to the GA carboxyl groups), was added to deionized water (1.5 mL). The GA and EDC solutions were mixed with continuous stirring at ambient temperature for 30 min to activate the carboxyl groups of GA. Subsequently, this mixture was added dropwise to the as-prepared CSMA solution. The pH of the mixture was adjusted to 5.0 with 1.25 M NaOH, followed by stirring at 25 °C in the dark for 24 h. Next, the resulting solution was dialyzed against hydrochloric acid (pH = 4) for 3 days to remove unreacted GA and prevent CSMAGA oxidation. This was followed by dialysis against deionized water for 12 h to remove HCl and other byproducts. Finally, the dialyzed solution was freeze-dried to obtain a CSMAGA derivative. The DS was calculated as follows:

$$DS = \frac{I_{7.26}/2}{I_{1.74\text{-}1.83}/3} \times 16.5\%, \quad (2)$$

where $I_{(7.26)}$ and $I_{(1.74–1.83)}$ denote the integrated areas of the benzene ring proton peak of GA at 7.26 ppm and the methyl proton peak at 1.74–1.83 ppm, respectively.

2.14. Characterization

^1H nuclear magnetic resonance (NMR) spectra of CS, CSMA, and CSMAGA were obtained on JNM-ECS400 (400 MHz; JEOL, Japan). Fourier transform infrared (FT-IR) spectra were recorded in the 4,000–600 cm^{-1} range on VERTEX-70 (Bruker, Germany). Ultraviolet (UV)-visible (UV–vis) absorption spectra were recorded in a UV-1800 spectrophotometer (Mapada, China).

2.15. Hydrogel fabrication

CSMA and CSMAGA were completely dissolved in aqueous LAP (2 mg/mL) at 20 mg/mL. The as-prepared precursor solutions were then irradiated with UV light (405 nm, 50 mW/cm^2) for 30 s for CSMA and CSMAGA hydrogel formation. Next, 10 mM MASM7 was added to the CSMAGA as-prepared precursor solution (1 mL), mixed ultrasonically, and irradiated with UV light (405 nm, 50 mW/cm^2) for 30 s to form the MASM7@CSMAGA hydrogel.

2.16. Scanning electron microscopy

CSMAGA and MASM7@CSMAGA hydrogels were cubed and lyophilized. Next, the cross-sections of the hydrogels were sprayed with a gold film to create a conductive environment, and hydrogels microstructure were observed on a Regulus-8100 scanning electron microscope (Hitachi, Tokyo, Japan) at an accelerating voltage of 15 kV.

2.17. Swelling test

The cylindrical hydrogels (height = 3 mm, diameter = 8 mm) were initially weighed (to obtain W_0) and then completely immersed in deionized water at 37 °C for 150 min (n = 3). At predetermined timepoints, the hydrogels were carefully removed and gently blotted with a filter paper to remove excess water. The swollen hydrogels were then weighed (to obtain W_1). The swelling ratio was calculated as follows:

$$\text{Swelling ratio} = \frac{W_1}{W_0} \times 100\% \quad (3)$$

In vitro hydrogel degradation was assessed in PBS containing lysozyme (30,000 FIP-U/mL) at 37 °C for 7 days. The PBS solution was refreshed every 2 days to ensure sustained enzyme activity. At predetermined intervals, the residual hydrogels were removed from the solution, carefully blotted with a filter paper to remove excess water, and weighed. The weight remaining ratio was calculated as follows:

$$\text{Weight remaining ratio} = \frac{W_1}{W_0} \times 100\% \quad (4)$$

2.18. Analysis of MASM7 release from MASM7@CSMAGA hydrogel

We prepared 1 mL of as-prepared precursor solution and irradiated it to obtain MASM7@CSMAGA hydrogel, as described in Section 2.14. The hydrogel was added to 5 mL of PBS (pH 7.4) with 10 % DMSO and maintained in an incubator with shaking (80 rpm) at 37 °C. At various predetermined timepoints, samples were withdrawn from the solution, which was immediately replenished with an equal volume of fresh PBS with 10 % DMSO to maintain constant conditions. The concentration of MASM7 released into the medium was quantified by measuring the samples' absorbance at 329 nm on a VICTOR NIVO multimode microplate reader (Revvity, Finland).

2.19. Hydrogel cytocompatibility

Cytocompatibility of our hydrogels was evaluated through direct contact between the hydrogels and DPSCs. In a 24-well plate, DPSCs were added to each well and incubated in a 5 % carbon dioxide atmosphere at 37 °C for 12 h to obtain a cell monolayer. Then, sterile hydrogels were placed in the wells, followed by incubation for 24 or 72 h. Next, cell viability was visually evaluated using a live/dead staining kit. Images were acquired under a fluorescence microscope (Zeiss, Germany). The cell viability and proliferation were also quantified using a cell counting kit 8 (CCK-8), where absorbance was measured at 450 nm on a luminometer plate reader (Molecular Devices, CA). Cells cultured without hydrogels were used as controls.

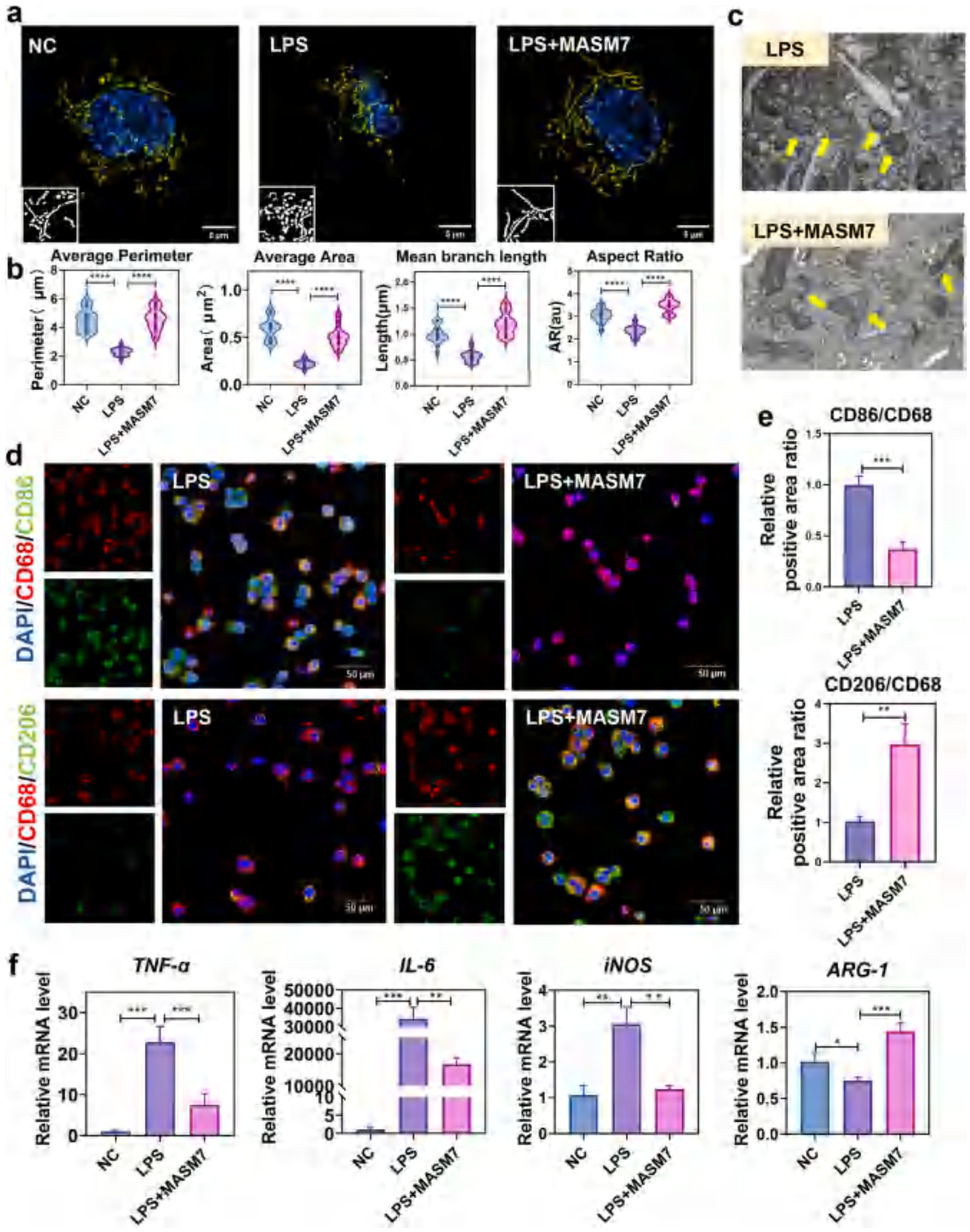

Fig. 1. MASM7 promotes the mitochondrial fusion of THP-1-M under inflammatory conditions and induces M2 polarization. (a) Mitochondrial images by super-resolution optical microscopy. The yellow color represents mitochondria. Scale bars, 5 μm. (b) Mitochondrial morphology analysis of average perimeter, average area, mean branch length and aspect ratio by MiNA in ImageJ software. The data are shown as the mean ± SD (n = 20); ****$p < 0.001$ indicate significant differences between the two groups. (c) Mitochondrial images by TEM. (d, e) Immunofluorescence showing the expression of polarization markers CD86, CD206 and CD68 in THP-1-M. The red color represents CD68 and the green color represents CD86 and CD206 respectively.Scale bars, 50 μm (f) qPCR analysis showing the expression of polarization-related cytokines *TNF-α*, *IL-6*, *iNOS* and *Arg-1*. The data are shown as the mean ± SD (n = 3); *$p < 0.05$, **$p < 0.005$ and ***$p < 0.001$ indicate significant differences between the two groups.

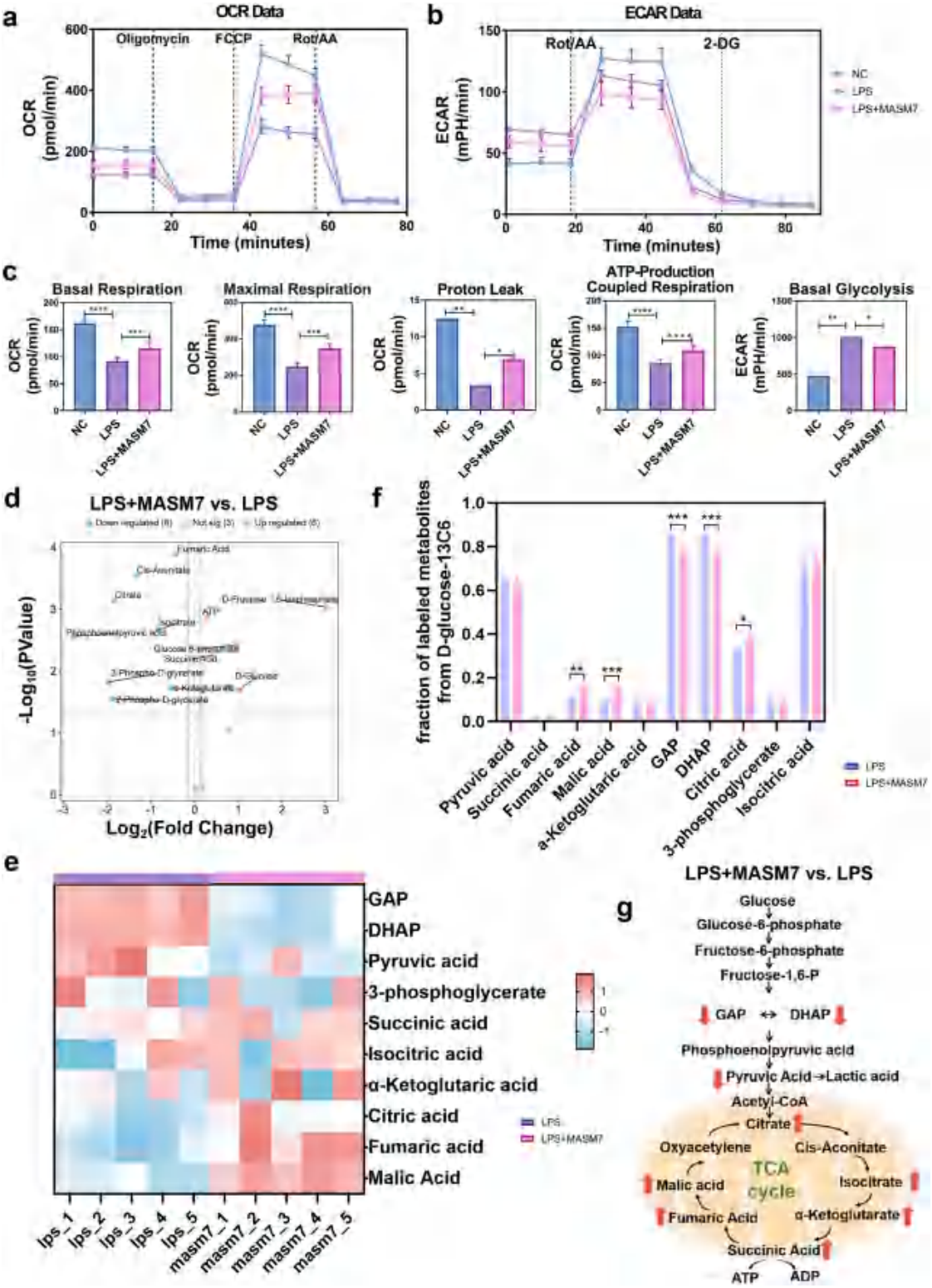

Fig. 2. MASM7 induces LPS-treated THP-1-M metabolic reprogrammig from glycolysis to OXPHOS. (a) OCRs of THP-1-M was measured in response to sequential treatment with Oligomycin, FCCP, and Rot/AA. (b) extracellular acidification rates (ECARs) of THP-1-M was measured in response to sequential injection with the addition of Rot/AA and 2-DG. (c) Quantification analysis of basal respiration, maximal respiration, proton leak, ATP-production coupled respiration and basal glycolysis. (d)Volcano plots of targeted metabolomics LC-MS data showing differentially abundant metabolites in glycolysis and TCA cycle in THP-1-M(the horizontal axis represents the direction and fold changes in metabolites, and the vertical axis represents the statistical significance of the change) for the LPS group vs. LPS + MASM7 group. (e) Heatmap of the MFA GC/MS data showing the abundance of labeling TCA cycle metabolites and labeling glycolysis metabolites in LPS group and LPS + MASM7 group. (f) Labeled extent of differently expressed TCA metabolites and glycolysis metabolites among the groups. (g) Schematic showing the changes in labeled key metabolites involved in glycolysis and the TCA cycle. The up (down) arrows indicate increases (decreases) in the levels of metabolites in LPS + MASM7group compared to that in LPS group. The data are shown as the mean ± SD (n = 3); *p < 0.05, **p < 0.005, ***p < 0.001 and ****p < 0.001 indicate significant differences between the two groups.

2.20. Hydrogel antioxidant activity assessment

The antioxidant ability of our hydrogels was assessed using the 1,1-diphenyl-2-picrylhydrazyl (DPPH) and 2,2-azino-bis (3-ethylbenzothiazoline-6-sulfonic acid) diammonium salt (ABTS) assays. The DPPH assay was performed using freshly prepared 2 mM DPPH/ethanol. In brief, crushed hydrogels (weight, 50 mg) were immersed in 3 mL of this DPPH for 30 min, centrifuged, and photographed. The supernatant's absorbance was measured at 519 nm. The electron paramagnetic resonance spectra were obtained between 3480 and 3570 G on an EMXplus EPR spectrometer (Bruker, Germany).

For the ABTS assay, crushed hydrogels (weight, 50 mg) were immersed in the ABTS solution for 30 min, centrifuged, and photographed. The supernatant's absorbance was measured at 714 nm. The electron paramagnetic resonance spectra were obtained between 3480 and 3560 G on an EMXplus EPR spectrometer (Bruker, Germany).

We also measured reactive oxygen species (ROS) levels in inflamed DPSCs in the presence of CSMA and CSMAGA by using an ROS assay kit (Beyotime, China) and CCK-8; 100 μM H_2O_2 was used to mimic oxidative stress under an inflammatory environment. DPSCs were seeded in confocal dishes and 96-well plates and then treated with PBS, CSMA, or CSMAGA along with H_2O_2 for 24 h. Next, the cells were incubated with 2′,7′-dichlorodihydrofluorescein diacetate (DCFH-DA) for 20 min and then washed with PBS. ROS was quantified on a confocal imaging system, and cell viability was measured on a microplate reader.

2.21. In vivo CSMAGA hydrogel degradation

To evaluate the in vivo degradation properties of CSMAGA hydrogel, Cy5.5 NHS ester (1 mg) was reacted with CSMAGA (0.1 g) in DMSO overnight. The resulting solution was then dialyzed in pure water for 2 days to remove unreacted Cy5.5 NHS ester. Next, the obtained Cy5.5-labeled CSMAGA precursor solution was completely dissolved in deionized water and filtered using a strainer (0.22 μm) to remove bacteria. The 30 μL of this as-prepared precursor solution was injected subcutaneously into the dorsal area of mice and allowed to gel in situ under UV irradiation. Hydrogel fluorescence was then monitored at different timepoints using an in vivo imaging system (Perkinelmer, USA) at appropriate wavelengths (λ_{ex} = 660 nm, λ_{em} = 710 nm).

2.22. Dental pulpitis rat model establishment

A pulpitis rat model was established, as described previously, with modifications [29,42]. In brief, 8-week-old male Sprague Dawley rats were anesthetized using peltorbarbitalum natricum intraperitoneally. Then, the maxillary first molar was drilled using a 1/4 round bur and cooled with 0.9 % normal saline. Pulpal exposure was confirmed and enlarged using a 25-K file with a 4 × loupe. The exposed pulp site was rinsed with 0.9 % normal saline, and sterile cotton wetted with 2 μL of 10 mg/mL LPS was placed on the pulp for 30 min. Thereafter, the exposed site was rinsed with 0.9 % normal saline again and then capped with capping materials. For the LPS group, MTA was used as the capping materials. For the CSMAGA group and MASM7@CSMAGA group, MASM7 was unloaded and loaded in 1 mL of the CSMAGA hydrogel, respectively; 2 μL of the hydrogel was used on each tooth. This was followed by irradiation with UV light (405 nm, 50 mW/cm^2) for 30 s.

Maxillary bones were collected 3, 7, and 14 days after pulp capping and then fixed with 4 % paraformaldehyde for 24 h. For histological and tissue immunofluorescence analyses, the tissues were sliced into 6-μm-thick sections and stained, as described previously [29,42].

2.23. Statistical analysis

We used independent two-tailed Student's *t* tests to compare data between two groups. One-way analysis of variance (ANOVA) was employed, followed by Tukey's post-hoc test, to compare differences among three or more groups. Data are presented as means ± standard deviation (SDs) from at least three independent experiments per group. A *P* value of <0.05 was considered to indicate statistical significance.

3. Results

3.1. MASM7 promotes mitochondrial fusion in THP-1-M cells under inflammation and orchestrates M2 polarization

LPS was used to mimic an in vitro inflammatory microenvironment to induce M1 macrophage polarization in THP-1-M cells (Fig. S1). The results demonstrated that the expression of mitochondrial fission-related markers was upregulated, whereas that of the mitochondrial fusion-related markers was downregulated, indicating an imbalance between mitochondrial fission and fusion. The morphological analysis revealed that the mitochondria of THP-1-M cells had become fragmented and swollen under LPS stimulation (Fig. S2). MASM7, a novel mitochondrial fusion activator, specifically bound to the HR-2 domain of MFN2 and efficiently promoted mitochondrial fusion. The super-resolution optical microscopy and TEM results demonstrated that MASM7 significantly restored the elongated morphology of LPS-altered mitochondria (Fig. 1a–c).

Next, we investigated the immunomodulatory effects of MASM7 on macrophage polarization phenotype. Immunofluorescence staining confirmed that compared with the LPS group, the MASM7+LPS group had fewer $CD68^+/CD86^+$ (M1 type) cells and more $CD68^+/CD206^+$ (M2 type) cells (Fig. 1d and e). LPS treatment increased the expression of the proinflammatory cytokines TNF-α, IL-6, and inducible nitric oxide synthase (iNOS); nevertheless, MASM7 treatment significantly reduced it. However, the expression of Arg-1, which is an anti-inflammatory marker, presented an opposite trend (Fig. 1f–S3).

In order to confirm the effect of MASM7, si-RNA of *MFN2* were used to down-regulated expression of MFN2(Fig. S4a and b), which leads to the loss of functional site of MASM7. Mitochondrial fusion induced by MASM7 couldn't be observed as that in normal condition (Fig. S4c). Then, immunofluorescence staining results showed that the $CD68^+/CD206^+$ (M2 type) cells were reduced in LPS + si-MFN2+MASM7 group (Fig. S4d) than that in LPS + MASM7 group.

Taken together, these results indicated that MASM7 can efficiently promote mitochondrial fusion in THP-1-M cells in an LPS-induced inflammatory microenvironment and that mitochondrial fusion caused by MASM7 can reduce the count of M1 macrophage but increase that of M2 macrophages; in other words, MASM7 can transform THP-1-M cells from its proinflammatory to anti-inflammatory state.

3.2. MASM7 leads to shifting of the main metabolic process from glycolysis to oxidative phosphorylation in THP-1-M cells under an inflammatory microenvironment

Mitochondria are the fundamental metabolic organelles in cells. Many studies have established metabolism and its associated metabolites as the key players in shaping macrophage phenotypes [43]. Moreover, THP-1-M cell polarization status is mainly modulated via changes in metabolic cascades due to mitochondrial fusion. To detect the mechanisms underlying MASM7 of THP-1-M cell polarization, we used the Seahorse assay to evaluate the OCR and ECAR, which represent oxidative phosphorylation (OXPHOS) and glycolysis, respectively. Fig. 2a and c illustrate OCR calculations based on sequential addition of 1.5 μM oligomycin, 1.5 μM FCCP, and 0.5 μM Rot/AA. The basal respiration rates of THP-1-M cells significantly decreased in the LPS group; nevertheless, they were restored after MASM7 treatment. After the addition of FCCP, the maximal respiration rate decreased in THP-1-M cells exposed to LPS; MSAM7 also reversed these changes. Moreover, LPS stimulation significantly reduced the proton leak rate and ATP-production coupled respiration rate in THP-1-M cells; nevertheless, they increased after MASM7 treatment. The basal glycolysis rate

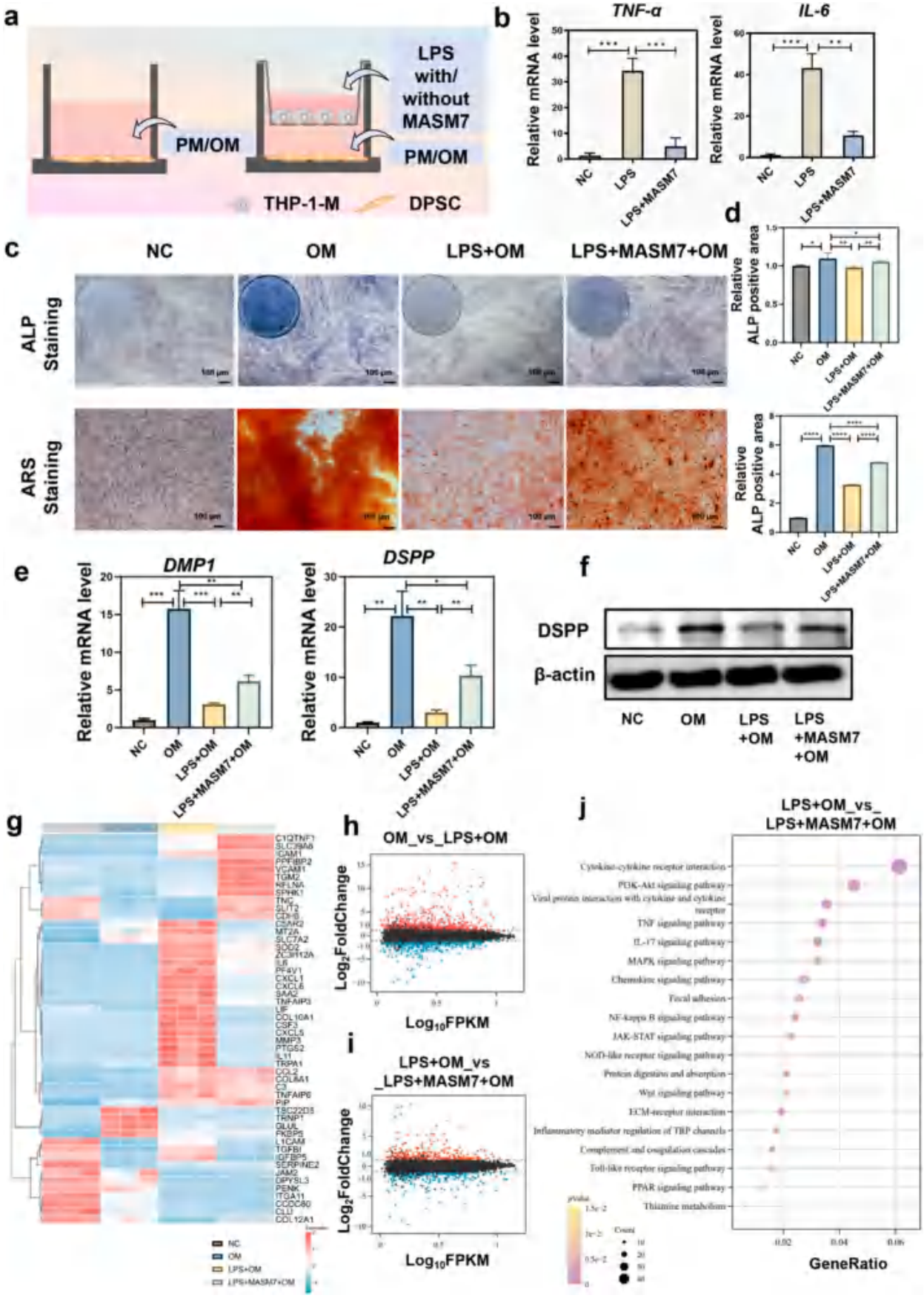

(caption on next page)

Fig. 3. The repair ability of DPSCs is enhanced by MASM7 treated THP-1-M under inflammatory microenvironments. (a) Schematic illustration of the co-culture system of THP-1-M and DPSCs. PM represents α-MEM medium supplemented with 10 % FBS and 1 % penicillin-streptomycin. OM represents the odontogenic medium. (b) qPCR analysis showing the expression of pro-inflammatory cytokines *TNF-α* and *IL-6* in DPSCs when co-cultured with THP-1-M after different stimulation. (c, d) ALP staining, ARS staining and relative positive area analysis in DPSCs under odontogenic medium (OM) when co-culterd with different treated THP-1-M. Scale bars, 100 μm. (e) qPCR analysis showing the expression of odontogenic markers *DSPP* and *DMP-1* in DPSCs under OM when co-culterd with different treated THP-1-M. (f) Western blot showing the expression of odontogenic markers DSPP. (g) Heatmap showing the top 50 changed genes abundance in DPSCs under OM when co-culterd with different treated THP-1-M. (h, i) The MA plot showing the differentially abundant gene in DPSCs for OM group vs. LPS + OM group (h), LPS + OM group vs. LPS + MASM7+OM group (i). (j) KEGG analysis between LPS + OM group vs. LPS + MASM7+OM group. The size of bubbles represents the number of differently expressed genes in the pathway. The color represents pValue of the pathway. The data are shown as the mean ± SD (n = 3); *p < 0.05, **p < 0.005, ***p < 0.001 and ****p < 0.001 indicate significant differences between the two groups.

(ECAR) was significantly higher in the LPS group than in the control group, which may be a compensatory mechanism for downregulated basal respiration. In contrast, MASM7 reduced the basal glycolysis rate in THP-1-M cells exposed to LPS (Fig. 2b and c).

We then performed targeted LC-MS to profile for metabolites involved in glycolysis and the TCA cycle in THP-1-M cells treated or not treated with LPS or MASM7. In total, 17 differential metabolites involved in glycolysis and the TCA cycle were identified between the LPS and LPS + MASM7 group; of them, six were significantly upregulated, whereas eight were significantly downregulated (Fig. 2d). The quantitative analysis (Fig. S5a) and heatmap (Fig. S5b) revealed changes in key metabolites of glycolysis and the TCA cycle. However, because changes in a single metabolite cannot reflect the promotion or inhibition of a metabolic process, we conducted ^{13}C-tracing MFA for further research(Fig. 2e and f). The results showed that the extent of ^{13}C labeled metabolites (the sum from M1 to M6) were changed during glycolysis and TCA cycle: labeled metabolomics from glycolysis (such as GAP, DHAP) were inhibited in the LPS + MASM7 group, whereas labeled metabolomics from TCA cycle(such as Fumaric acid, Malic acid, Citric acid) were upregulated. It represents that MASM7 enhanced OXPHOS and reduced glycolysis under inflammatory microenvironment. We plotted a flow diagram of all key metabolites to present the shifting trend and positions in glycolysis and the TCA cycle(Fig. 2g). In general, glycolysis was inhibited in the LPS + MASM7 group, whereas OXPHOS was upregulated. Taken together, these results indicated that MASM7 can lead to metabolic reprogramming in THP-1-M cells under an inflammatory microenvironment, shifting the main metabolic process from glycolysis to OXPHOS.

3.3. MASM7-treated THP-1-M cells enhance repair ability of DPSCs under an inflammatory microenvironment

DPSCs, crucial stem cells in the dental pulp tissue repair process, can be influenced by macrophage polarization in inflammatory microenvironments. The expression of inflammatory markers and odontogenesis-related markers in DPSCs is a useful index to assess their repair ability. To detect the role of LPS- or LPS + MASM7-treated THP-1-M on DPSCs, we cocultured DPSCs and THP-1-M as shown in Fig. 3a. The qPCR results (Fig. 3b) demonstrated that the expression of the proinflammatory cytokines *TNF-α* and *IL-6* was upregulated in DPSCs cocultured with LPS-stimulated THP-1-M cells. Nevertheless, coculture with MASM7-treated LPS-stimulated THP-1-M significantly downregulated the expression of these cytokines in DPSCs. Next, we added OM to the cocultured system to explore the odontogenesis ability of DPSCs under an inflammatory microenvironment. ALP staining (Fig. 3c and d) revealed that at day 3, ALP expression was inhibited in DPSCs cocultured with LPS-stimulated THP-1-M cells; nevertheless, this condition was reversed after MASM7 treatment. ARS staining, which reflects mineralized nodule formation, was performed 14 days after coculture, and its results concurred those of ALP staining. We then measured changes in DSPP and DMP-1, which are specific odontogenesis markers in DPSCs at the late stage. The results demonstrated that DSPP and DMP-1 expression was higher in DPSCs cocultured with LPS + MASM7-treated THP-1-M cells than in those cocultured with LPS-stimulated THP-1-M cells (Fig. 3e and f). These results indicated that THP-1-M cells under an inflammatory microenvironment can reduce the repair ability of DPSCs and that MASM7 can reverse this effect to a certain extent. To reinforce translational value, hPBMDM were used to co-culture with DPSCs. The results (Figs. S6a, b, c)showed that ALP expression and mineralized nodule formation were up-regulated in DPSCs when co-cultured with MAMS7-stimulated hPBMDM under inflammatory microenvironment than that in LPS group. What's more, the expression of DSPP was also increased in LPS + MASM7 group (Fig. S6d).

We then used RNA sequencing to explore the transcriptomic changes in the cocultured DPSCs with THP-1-M cells. A heatmap (Fig. 3g) of the cluster analysis of significantly changed genes in different groups was plotted. An MA map was used to present the distribution of changed genes between the OM and OM + LPS groups (Fig. 3h) or between the OM + LPS and OM + LPS + LPS groups (Fig. 3i). The results demonstrated that IL-6 expression was higher in the OM + LPS group than in the OM group but lower in the OM + LPS + MASM7 group. The expression of ALP, an odontogenesis-related marker in the early stage, was higher in the OM + LPS + MASM7 group than in the OM + LPS group. This result was also consistent with ALP staining. KEGG pathway enrichment analysis (Fig. 3j) demonstrated that most of the genes differently expressed between the OM + LPS and OM + LPS + MASM7 groups were related to inflammatory pathways such as the PI3k-Akt and NF-κB pathways, as well as tissue repair and regeneration pathways, such as the MAPK, JAK-STAT, and Wnt pathways.

3.4. CSMAGA demonstrates good injectability, antioxidant ability and biocompatibility

We selected CS as the macromolecular skeleton to prepare our hydrogel scaffold for tissue repair because of its intrinsic biocompatibility and biodegradability. To endow CS with both rapid photocuring and good antioxidant ability for scavenging free radicals during pulpitis, the carbon–carbon double bond and pyrogallol group were covalently linked to the CS backbone via an acylation reaction and an EDC-catalyzed coupling reaction (Fig. S7a). The precise chemical structure of CS derivatives was confirmed using ^{1}H NMR spectroscopy (Fig. 4a). CS, CSMA, and CSMAGA displayed a characteristic peak at 1.74–1.83 ppm (9, 3H), corresponding to the protons of methyl groups from N-acetylglucosamine of the CS backbone and signals between 3.15 and 3.84 ppm due to protons of the glucosamine ring (3-4-5-6, 5H). Compared with native CS, CSMA and CSMAGA revealed two newly formed characteristic peaks at 5.45–5.85 ppm, corresponding to methylene protons (7, 2H), demonstrating the successful covalent linkage of the carbon–carbon double bond group onto the CS backbone. The DS of the carbon–carbon double bond group in CSMA and CSMAGA was 32 %. Compared with native CS and CSMA, CSMAGA revealed a newly formed characteristic peak at 7.26 ppm corresponding to benzene ring protons, indicating the effective covalent linkage of the pyrogallol group onto the CS backbone. The DS of the pyrogallol group in CSMAGA was 2 %. In the FT-IR spectra of CSMAGA, two new characteristic absorbance bands at 1537 and 1220 cm^{-1}, corresponding to –OH (pyrogallol group) and C–O/C–C stretching vibrations, respectively, were observed (Fig. 4b). These results indicated that the pyrogallol group was effectively linked to CS; however, the other functional groups of native CS remained unaffected.

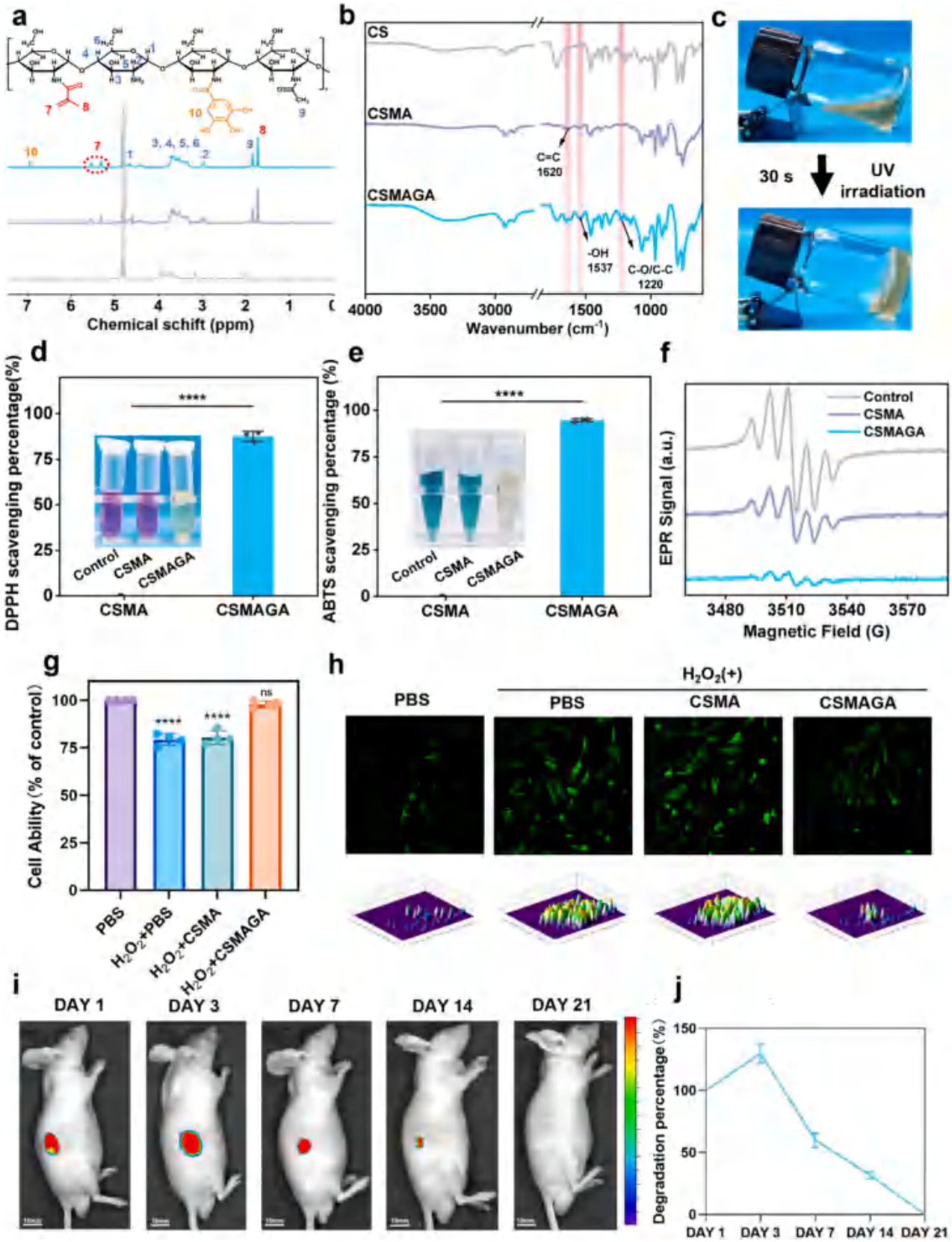

Fig. 4. Synthesis and characterization of CSMA and CSMAGA. (a)^{1}H NMR spectra of CS, CSMA and CSMAGA. (b) FT-IR results of CS, CSMA and CSMAGA. (c) Optical images showing the photo-cross-link ability of CSMAGA. (d, e) Optical color shifting and data analysis of DPPH and ABST radicals. (f) The EPR result of DPPH. (g) CCK-8 result showing DPSCs viability under 100 μM H_2O_2 with or without different hydrogels on 24 h. (h) Representative ROS staining images and three-dimensional surface plot images of DPSCs under 100 μM H_2O_2 with or without different hydrogels on 24 h. ROS was probed by DCFH-DA. The data are shown as the mean ± SD (n = 3); ****p < 0.001 indicate significant differences between the two groups.

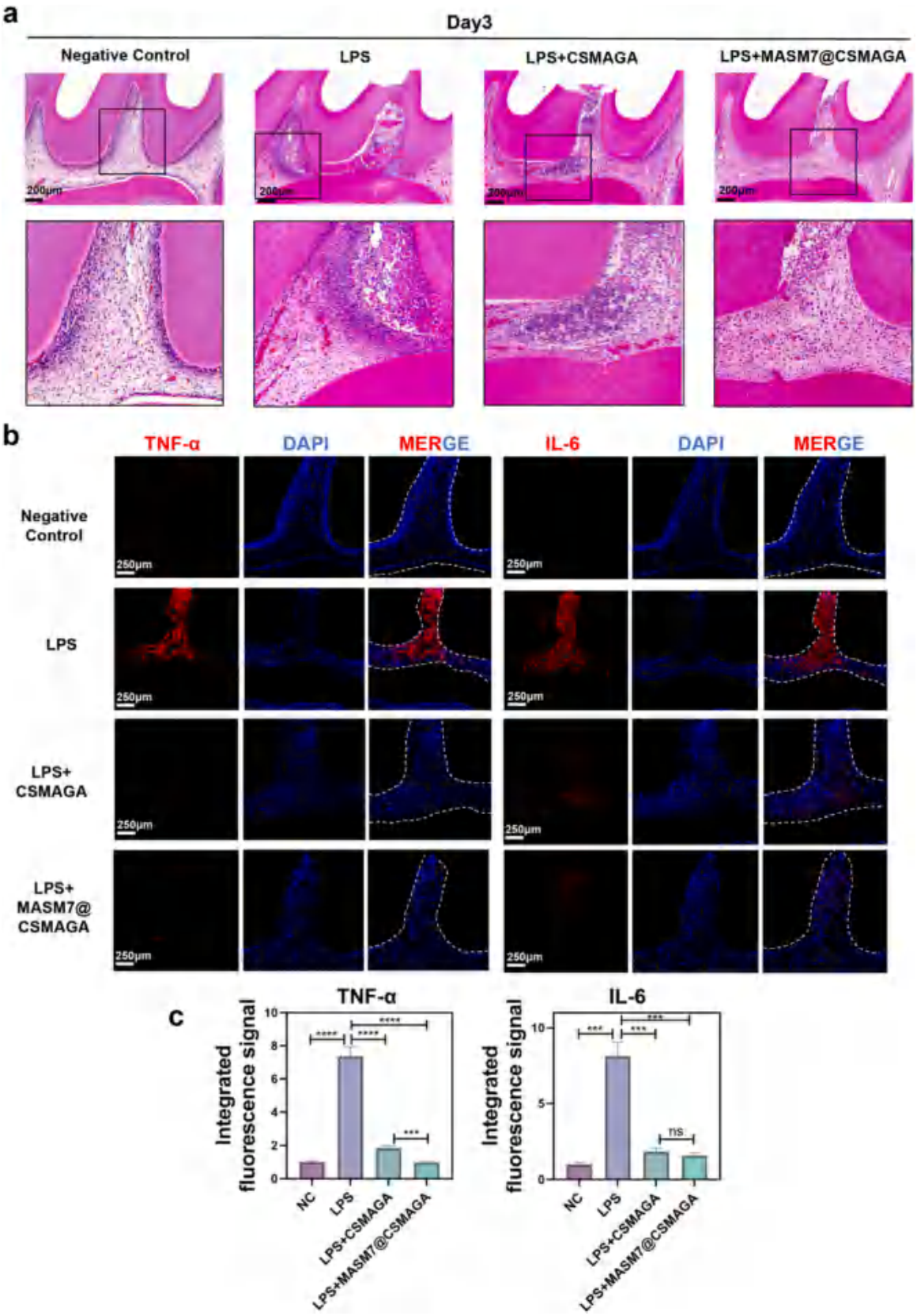

Fig. 5. The inflammatory levels in pulpitis model of rats on Day 3. (a) H&E staining showing inflammatory cell infiltration in LPS-induced pulpitis in rats after different treatment on day 3. Scale bars, 200 μm. (b, c) Immunofluorescence staining(b) and integrated fluorescence signal analysis(c) for the expression of inflammatory markers TNF-α and IL-6 at the site of pulp injury after treatment on day 3. The area surrounded by white dashed line represents pulp tissue. Scale bars, 250 μm ***$p < 0.001$ and ****$p < 0.001$ indicate significant differences between the two groups.

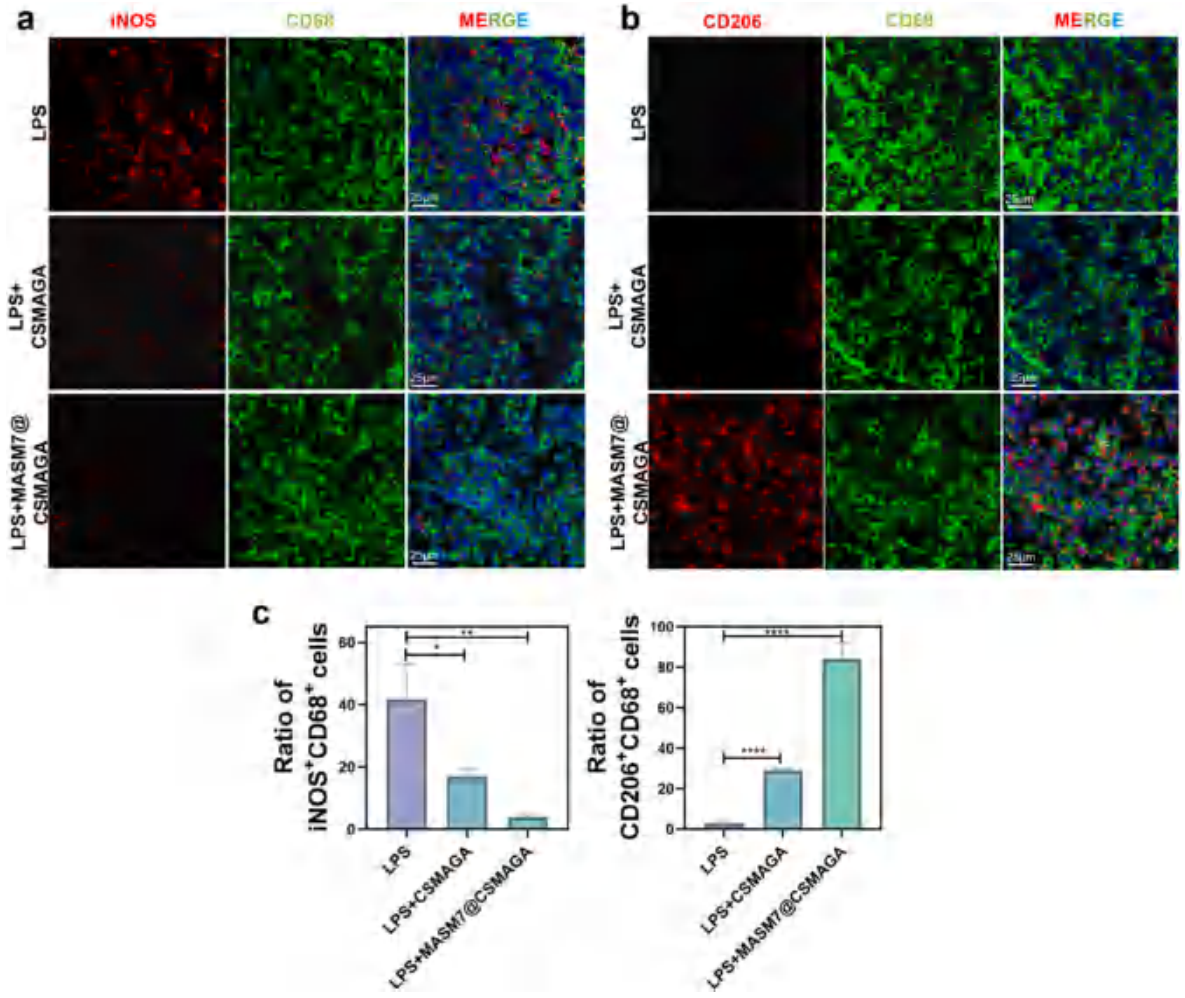

Fig. 6. MASM7@CSMAGA hydrogel induces immune modulation in pulpitis model. (a) Immunofluorescence staining showing the M1 polarization-related markers (iNOS/CD68) at the site of pulp injury after treatment on day 3. The red color represents iNOS and the green color represents CD68. (b) Immunofluorescence staining showing the M2 polarization-related markers (CD206/CD68) at the site of pulp injury after treatment on day 3. The red color represents CD206 and the green color represents CD68. (c) Statistical analysis of the numbers of M1 macrophages (CD68+iNOS + cells) and M2 macrophages (CD68+CD206+cells). Scale bars, 25 μm *p < 0.05, **p < 0.01, and ****p < 0.001 indicate significant differences between the two groups.

CSMAGA exhibited strong UV absorption at 268 nm, attributable to electron transfer from nonbonding π orbitals to antibonding π* orbitals of the benzene ring of the pyrogallol group (Fig. S7b). Under UV irradiation at 405 nm for 30 s, CSMAGA precursor solution at 20 mg/mL rapidly transformed into a stable hydrogel (Fig. 4c). The CSMAGA precursor solution could be continuously extruded through a needle, confirming the injectability and wound shape adaptability of the hydrogel (Fig. S7g). Our CSMAGA hydrogel also appeared to have a suitable swelling performance (Fig. S7c), indicating its ability to effectively absorb water without becoming structurally unstable. Compared with our CSMA hydrogel, our CSMAGA hydrogel exhibited a higher swelling ratio (≈190 %) after immersion in deionized water for 150 min. The swelling ratio was higher due to the pyrogallol group, which features a profusion of phenolic hydroxyl groups. Within 7 days of exposure to lysozyme, our CSMA hydrogel became degraded by 63 %, whereas our CSMAGA hydrogel became completely degraded (Fig. S7d). SEM images revealed the porous structure of our CSMAGA hydrogel and MASM7@CSMAGA hydrogel (Fig. S7e). As illustrated in Fig. S7f, the MASM7@CSMAGA hydrogel exhibited drug delivery ability of MASM7, with the cumulative release rate reaching 80 % after 24 h of incubation.

The antioxidant activity of hydrogels was first assessed using DPPH and ABTS free radicals. At 37 °C, the CSMAGA hydrogel changed the color of the DPPH solution from dark purple to yellow, whereas it changed the color of the ABTS solution from blue to gray. This color shift indicated the hydrogel's ability to effectively remove both DPPH and ABTS free radicals (Fig. 4d and e). The DPPH and ABTS assay results indicated that the CSMAGA hydrogel eliminated >80 % of the DPPH and ABTS radicals, respectively. Similarly, the EPR spectra (Fig. 4f–S4h) demonstrated that the DPPH and ABTS free radical peak intensity decreased after CSMAGA hydrogel treatment. These results confirmed that our CSMAGA hydrogel has substantial free radicals scavenging efficacy. To confirm the anti-oxidative ability of our CSMAGA hydrogel, we cultured DPSCs with 100 μM H_2O_2 to mimic an oxidative stress condition and then treated them with our CSMA or CSMAGA hydrogel. CCK-8 assay revealed that the CSMAGA hydrogel considerably rescued DPSCs from oxidative damage-induced cell death (Fig. 4g). Intracellular ROS probing revealed that the CSMAGA hydrogel significantly reduced ROS levels and effectively attenuated oxidative stress (Fig. 4h).Taken together, these results indicated the substantial antioxidant ability of our CSMAGA hydrogel through RNOS scavenging.

Live/dead cell staining revealed that most DPSCs were live (green fluorescence) within the CSMA and CSMAGA hydrogel groups over time; very few dead cells (red fluorescence) were observed (Fig. S8a). Furthermore, DPSCs cultured directly with our CSMA or CSMAGA hydrogel demonstrated >90 % viability, indicating excellent cytocompatibility of both hydrogels. DPSC proliferation was observed in all

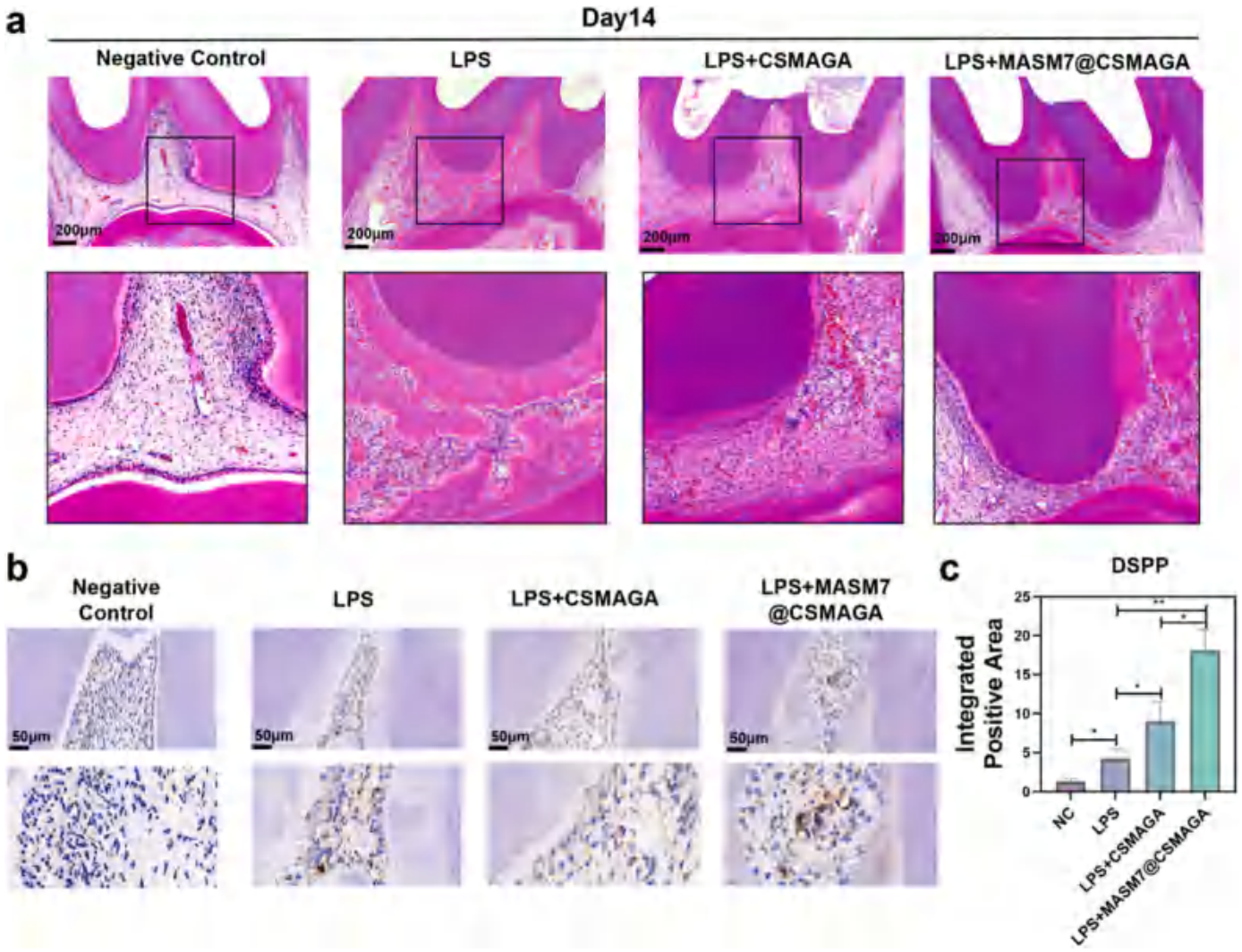

Fig. 7. MASM7@CSMAGA promotes the repair of pulpitis. (a) H&E staining showing the repair of pulp tissue on day14. Scale bars, 200 μm. (b) immunohistochemical staining showing the expression of odontogenic specific markers DSPP at the injury site of pulp tissue on day14. Scale bars, 50 μm.(c) Integrated positive area analysis of DSPP on day 14. *p < 0.05, **p < 0.005 indicate significant differences between the two groups.

groups, corroborating our live/dead cell staining results (Fig. S8b). Then, we prepared a leach liquor from MASM7@ CSMAGA and evaluated its biological activity on DPSCs when co-cultured with THP-1-M cells under inflammatory conditions. As shown in the supplementary data (Fig. S9), MASM7@CSMAGA hydrogel exhibited same biological effects comparable to those in the MASM7 group. The extent of ARS mineralization in the MASM7@CSMAGA and the MASM7 group was similar to that of the OM control group, with no significant difference (Fig. S9a and c). Furthermore, Western Blot analysis confirmed that the expression of DSPP was similarly in OM group, MASM7 group and MASM7@CSMAGA group (Fig. S8d).

These results indicated that both CSMA and CSMAGA hydrogels have high cytocompatibility and support cell proliferation, demonstrating their suitability for pulpitis treatment. In vivo fluorescence imaging revealed that Cy5.5 NHS ester-labeled CSMAGA hydrogel degraded in the subcutaneous tissue of mice within 21 days of administration (Fig. 4i and j).

3.5. MASM7@CSMAGA hydrogel exhibits dual effects of immunoregulation and antioxidation to promote inflamed pulp repair in rats

Next, we assessed whether our MASM7@CSMAGA hydrogel exhibits immunoregulatory and antioxidant effects on inflamed pulp in rats with dental pulpitis; the experimental design and model establishment process are presented in Fig. S10. Organ toxicity of our hydrogels was analyzed using hematoxylin and eosin (H&E) staining (Fig. S8c). The results demonstrated that on treatment day 3, the CSMAGA and MASM7@CSMAGA hydrogels reduced the infiltration of inflammatory cells in the maxillary first molar compared with the LPS group; nevertheless, the MASM7@CSMAGA hydrogel had a stronger effect than the CSMAGA hydrogel (Fig. 5a). We also performed immunofluorescence staining for the proinflammatory cytokines TNF-α and IL-6 to reflect the oxidative stress-induced inflammation levels in the rat dental pulp tissue. The results demonstrated lower cytokine levels in the CSMAGA hydrogel group than in the LPS group, indicating a substantial antioxidant effect of the hydrogel (Fig. 5b and c). To examine the immunoregulatory effects of our MASM7@CSMAGA hydrogel, we assessed the polarization states of macrophages around the inflamed pulp area through immunofluorescence staining for M1 and M2 polarization markers (iNOS and CD206, respectively), as well as the specific macrophage marker CD68. The results (Fig. 6a and b) revealed more $CD68^{+}iNOS^{+}$ cells (M1 macrophages) in the tissue from the LPS group. Nevertheless, the MASM7@CSMAGA hydrogel was noted to significantly reduce the number of these cells but increase that of more $CD68^{+}CD206^{+}$ cells (M2 type macrophages). These results indicated

that MASM7 delivered via the CSMAGA hydrogel had the immunoregulatory effect through modulation of the M2-to-M1 polarization of macrophages. Next, we evaluated inflamed pulp repair by assessing new dentin formation through H&E staining and DSPP expression through immunohistochemical staining. The H&E staining results on treatment day 14 (Fig. 7a) showed that new dentin formed in all three groups. Moreover, both the LPS and MASM7@CSMAGA hydrogel groups demonstrated dentin bridge formation around the exposed pulp area; in the CSMAGA hydrogel group, however, dentin bridge formation was delayed, yet slight inflammatory cell infiltration was observed. However, the LPS group also demonstrated extensive calcification in some areas of the pulp tissue, potentially due to chronic inflammatory stimulation; calcification typically was not expected to happen during the inflamed dental pulp repair process. Immunohistochemical staining (Fig. 7b and c) revealed higher DSPP expression in the CSMAGA and MASM7@CSMAGA hydrogel group than in the LPS group. Notably, the DSPP-positive area was larger in the CSMAGA hydrogel group than in the LPS group, possibly because new dentin had already formed in the LPS group and the expression of DSPP was decreased.

4. Discussion

Vital pulp therapy, typically used to treat pulpitis, avoids the complete removal of pulp tissue by applying biologic pulp capping materials [44]. Its effectiveness depends on two pivotal factors: prompt control of pulp inflammation and amelioration of the inflammatory microenvironment. In recent years, modulating host immune response to control inflammation has become a main focus in tissue repair and regeneration. Inducing M2 polarization in macrophages is a common method used for host immune regulation [45]. Furthermore, ROS in inflammatory microenvironments can cause oxidative stress [46]. Scavenging ROS to ameliorate such microenvironments in inflamed pulp is also crucial for pulp tissue self-repair [22]. The efficacy of current clinically used pulp capping materials mostly depends on the strong alkalinity of the materials themselves and the release of calcium ions, both of which promote tissue repair and regeneration. However, these materials may cause ectopic calcification within pulp tissue [47]. Recent studies have reported a series of pulp capping materials focused on immuno-regulation effect [48,49] or ROS scavenging [22,50] separately, rarely has any report simultaneously addressed both of these effects. Consequently, in the current study, we analyzed and confirmed the performance of MASM7, a small-molecule “mitochondrial glue”, in mediating the M2 polarization of macrophages via promotion of mitochondrial fusion under inflammatory conditions. We then loaded MASM7 onto a photo-cross-linkable CS hydrogel modified with GA to form MASM7@CSMAGA, a dual-effect hydrogel with immunoregulatory and antioxidant capacities. This hydrogel is injectable with in situ gelling properties, making it precisely fit the irregular shape of inflamed pulp tissue under different conditions.

Macrophage polarization is orchestrated by various signaling pathways, such as the NF-κB and JAK/STAT pathways, and cytokines such as interferon (IFN) γ and IL-4 [16,51]. M2 macrophages can form either via M0 macrophage polarization or through M1 macrophage repolarization. In inflammatory environments, such as pulpitis, macrophage polarization toward the M1 type increases [8,48]. As such, the repolarization of M1 macrophages to the M2 type under inflammatory conditions is crucial. However, the plasticity of M1 macrophages is often hindered under such inflammatory conditions [11,52]. The conventional pro-M2 polarization cytokine IL-4 cannot induce the transformation of M1 macrophages to the M2 type, primarily because of impaired mitochondrial function in M1 macrophages, which impacts their ability to repolarize considerably. Enhancing mitochondrial function can effectively recover the repolarization capacity of M1 macrophages to the M2 type [53]. Mitochondrial dynamics, a mitochondrial quality control component, can modulate mitochondrial function, making it a feasible process for regulating macrophage polarization [54]. In the current study, we pretreated THP-1-M cells with LPS in vitro to mimic the inflammatory milieu of pulpitis. This stimulation led to a considerable increase in M1 polarization—a finding that aligns with previous in vivo observations. We noted that macrophages subjected to inflammatory conditions exhibit higher mitochondrial fission marker expression but lower mitochondrial fusion marker expression, which leads to mitochondrial fragmentation. This result has also been confirmed in macrophage lines other than THP-1 cells [55]. As such, here, we proposed using MASM7, a mitochondria fusion promoter designed via computer screening, to induce M2 polarization in macrophages under inflammatory conditions. First, we confirmed that MASM7 promotes mitochondrial fusion in THP-1-M cells under inflammatory conditions. The super-resolution optical microscopy and TEM results both indicated that MASM7 induces an elongated mitochondrial morphology with normal cristae structure in LPS-pretreated THP-1-M cells, in contrast to the fragmented and swollen state observed after LPS treatment. Subsequently, we investigated whether MASM7 induces M2 polarization in LPS-pretreated macrophages and found that MASM7 increased M2 polarization marker expression but reduced that of M1 polarization markers, indicating that MASM7 effectively promotes macrophage polarization towards the M2 type in inflammatory microenvironments.

Mitochondrial functions are closely related to cellular metabolism, and OXPHOS occurs in mitochondria [56]. When the mitochondrial fission rate increases, cells predominantly depend on glycolysis for energy; in contrast, OXPHOS emerges as the chief metabolic pathway when the mitochondrial fusion rate increases [12,57]. Cellular metabolic reprogramming has a key regulatory role in finetuning macrophage polarization. We found that after LPS stimulation, macrophages exhibited a significant increase in the glycolysis rate, along with a decrease in the OXPHOS rate. Nevertheless, MASM7 reversed these changes: the OXPHOS rate increased, whereas the glycolysis rate decreased; this indicated that metabolic reprogramming had occurred in these cells. To further elucidate the specific changes in the metabolites during this process, we performed targeted metabolomic analysis for various glycolysis and TCA cycle metabolites. The results demonstrated that the levels of many glycolysis and TCA cycle metabolites were altered. However, changes in metabolites do not reflect as genetic changes because a metabolic process results from a series of product changes, known as metabolic flux [58]. In other words, an increase or decrease in the levels of a particular metabolite does not necessarily indicate the upregulation or downregulation of a metabolic pathway. As such, we conducted MFA to detect the real changes of metabolites in glycolysis and TCA cycle. Interestingly, some metabolites in TCA cycle showed different change tendency in the results of targeted metabolism and MFA. The reason may be that after treatment of MASM7, the metabolic flux of the TCA cycle was accelerated. However, these TCA metabolites did not accumulate within the cells (as indicated by metabolomics data). Instead, they were rapidly consumed through OXPHOS, resulting in the production of CO_2 for excretion, and were also utilized for the synthesis of other cellular components. Thus, LPS treatment may impede mitochondrial function in macrophages, hindering the TCA cycle. MASM7 can promote mitochondrial fusion, then reverse mitochondrial effect and enhance the TCA cycle. Collectively, these observations indicated that MASM7 can promote mitochondrial fusion and shift the metabolic mode from glycolysis-dominant to OXPHOS-dominant in LPS-pretreated macrophages, facilitating macrophage polarization toward the M2 type.

DPSCs, characterized by their multipotent differentiation capabilities, are key cells in pulp repair after pulpitis. The cytokines secreted by macrophages after polarization exert considerable regulatory effects on the reparative capacity of DPSCs. Subsequently, we devised a DPSC–THP-1-M cell coculture system to investigate the effects of THP-1-M cells treated with MASM7 under inflammatory conditions on DPSCs. In this system, THP-1-M cells and DPSCs were cultured in the upper and lower chambers of a transwell plate, respectively. This allowed the cytokines secreted by the THP-1-M cells under varying conditions to be

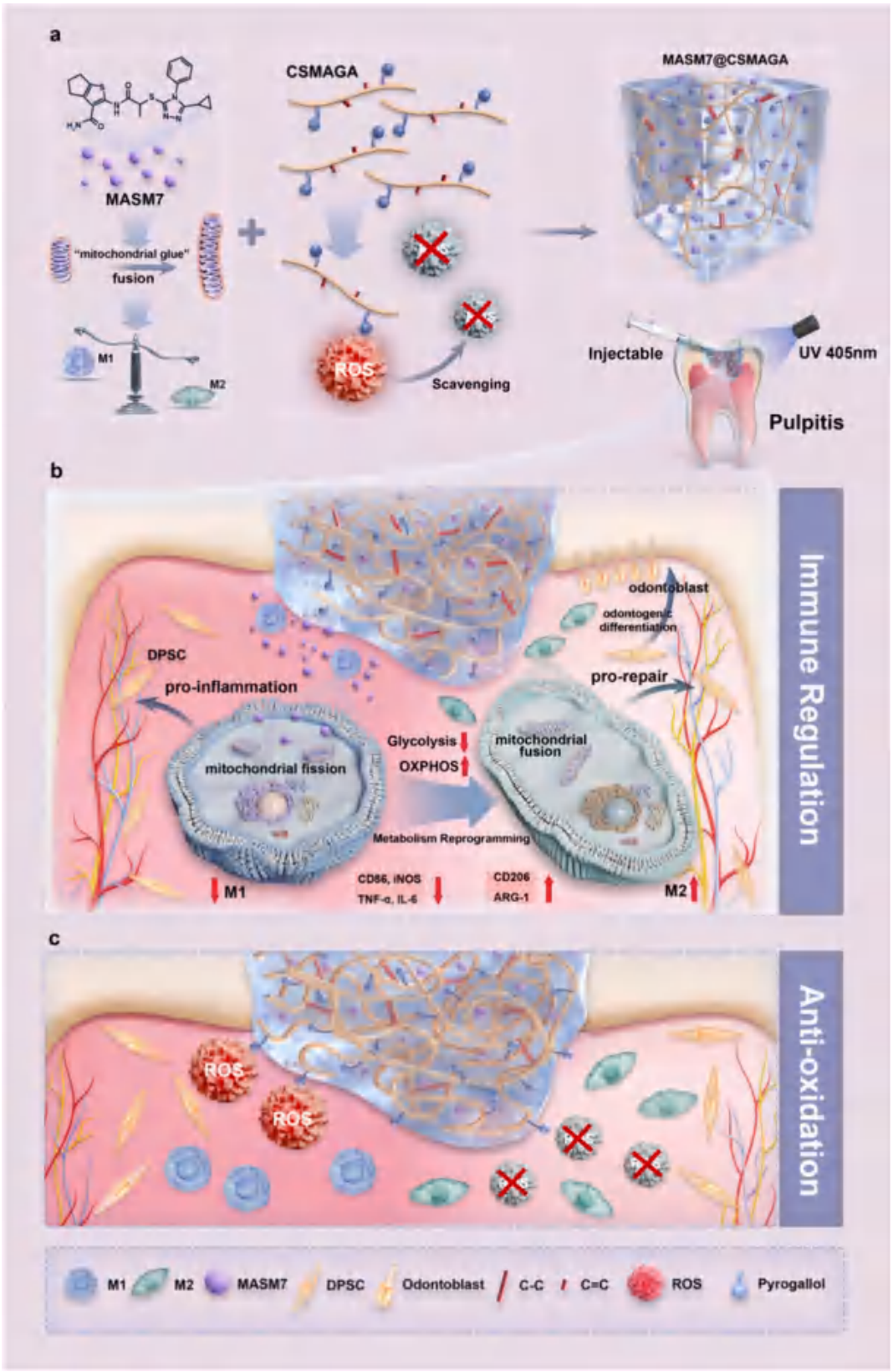

Fig. 8. Illustration of the synthesis and mechanism of the dual-effect hydrogel with immune regulation and antioxidant ability in pulpits. (a) Schematic showing the synthesis of the dual-effect hydrogel with immune regulation and antioxidant ability. (b) The underlying mechanism of "immune regulation" in macrophages by the hydrogel. (c) The process of "anti-oxidation" in inflammatory pulp tissue by the hydrogel.

transported to the lower chamber through the microporous membrane of the plate to act on the DPSCs. The results demonstrated that coculture with LPS-pretreated THP-1-M cells led to an upregulation of several proinflammatory cytokines in DPSCs. Nevertheless, exposure of LPS-pretreated THP-1-M cells to MASM7 downregulated the expression of these proinflammatory cytokines in DPSCs. Thus, macrophage polarization may modulate the inflammatory status of DPSCs, with MASM7 as a key factor in this modulation. We then assessed the odontogenic differentiation potential of DPSCs after coculture with THP-1-M cells. The findings demonstrated that macrophages under inflammatory conditions inhibited ALP production and mineralized deposition via DPSCs. Nevertheless, MASM7 treatment increased the expression of these markers. The expression of DSPP and DMP-1, key pulp repair proteins, demonstrated considerable increase in DPSCs after coculture with MASM7-treated THP-1-M cells under an inflammatory microenvironment. Thus, MASM7 can induce macrophages under inflammatory conditions to polarize toward the pro-repair type M2. To reinforce translational value, hPBMDM were also used to co-culture with DPSCs, and promote the repair ability of DPSCs.

To further elucidate the genomic changes and mechanisms in DPSCs during the repair process in the early stage, we performed RNA sequencing of the cocultured DPSCs. The results demonstrated that MASM7 treatment of LPS-pretreated THP-1-M cells downregulated the expression of proinflammatory cytokines, such as *IL-6*, in DPSCs—consistent with our qPCR findings (Fig. 3b). Moreover, it induced changes in the expression of various chemokines and angiogenesis-related factors in DPSCs, suggesting that DPSCs were positively engaged in the tissue repair process [59]. KEGG pathway enrichment analysis revealed that in addition to inflammation-related pathways such as the NF-κB and PI3k-Akt pathways [60,61], tissue repair-related pathways, including the MAPK and Wnt pathways [62,63], were significantly altered.

After completely validating the regulatory effects of MASM7 on macrophage polarization toward the M2 type and its impact on DPSCs' repair capacity, we designed a photo-cross-linkable CS hydrogel with antioxidant properties to deliver MASM7, which could exert immunoregulatory and antioxidant effects in inflamed dental pulp locally and thus facilitate its repair. In a pulpitis microenvironment, oxidative stress can damage local cells and impair tissue repair efficacy [22]. Recently, CS hydrogels have been applied in pulp repair; however, they have some limitations when applied to inflamed pulp tissue: most CS hydrogels can either be used only as a drug delivery system or lack rapid in situ gel-forming properties, making them unable to adapt to different pulp tissue injury morphologies. Therefore, to address these issues, we introduced MA into the CS hydrogel to synthesize a CSMA hydrogel, with photo-cross-linking properties. We then modified it further with GA to obtain a CSMAGA hydrogel, with photo-cross-linking and antioxidant properties. GA's pyrogallol group enables this hydrogel to effectively scavenge various free radicals through electron or proton transfer, thereby reducing the damage caused by free radicals to cells in inflammatory microenvironments. Moreover, being injectable, the hydrogel can conform precisely to the unique shape of each pulp injury. We also confirmed the biocompatibility, and degradability of our CSMAGA hydrogel, establishing a strong foundation for its local application in inflamed dental pulp repair.

Pulpitis is caused by bacterial infection, and the bacterial endotoxin LPS is key in its pathogenesis. Various methods have been used to establish pulpitis rat models, such as stimulating exposed pulp tissue with LPS or feeding a cariogenic diet followed by bacterial application [8,29,64,65]. However, based on ethical considerations and the need for a consistent pulpitis model, we simulated inflammation in rat pulp by using LPS in this study. Subsequently, we applied our dual-effect hydrogel to the injury locally and assessed its effects on pulp repair. Proinflammatory factor expression is essential to reflect oxidative stress levels in tissues. At 3 days after treatment, proinflammatory factor expression in the pulp tissue was significantly weaker in the CSMAGA hydrogel group than in the LPS group, indicating that the hydrogel had exerted its antioxidant stress effect. The expression of inflammatory factors in the MASM7@CSMAGA hydrogel group further decreased compared with the CSMAGA hydrogel group, suggesting that MASM7-induced M2 polarization in macrophages might play a regulatory role at this timepoint. Subsequently, the resulting direction of macrophage polarization confirmed our hypothesis. In addition, we examined the inflamed pulp repair outcome 14 days after treatment. After the application of the traditional pulp capping material, MTA, calcified tissue was diffusely distributed in the pulp chamber, which is not an ideal healing result. However, in the MASM7@CSMAGA hydrogel group, new dentin formation was observed on the injury surface, and no diffuse calcified tissue was found inside the treated tissue.

5. Conclusion

We developed MASM7@CSMAGA hydrogel with immunomodulatory and antioxidant abilities, which can accelerate inflamed pulp tissue repair after pulpitis (Fig. 8a). MASM7 promoted mitochondrial fusion to modulate THP-1-M polarization shifting to M2 type under inflammatory conditions with macrophages underwent metabolic reprogramming, the key energy-generating pathway changing from glycolysis to OXPHOS. Moreover, coculture with MASM7-treated THP-1-M cells enhanced the repair ability of DPSCs under inflammatory conditions (Fig. 8b). Our CSMAGA hydrogel was injectable and biocompatible and could deliver MASM7. Notably, the hydrogel exerted antioxidant effects by scavenging ROS (Fig. 8c).

In general, we presented a promising strategy for vital pulp preservation during pulpitis treatment, with emphasis on promoting M2 macrophage polarization through mitochondrial fusion under inflammatory conditions. In the future, MASM7 may be used to treat other diseases requiring immunoregulation-based treatment and we plan to further investigate the *ex vivo* human pulp tissue explants or dental pulp organoid to achieve the clinical use of the hydrogel.

CRediT authorship contribution statement

Dan Wang: Writing – original draft, Methodology, Investigation, Funding acquisition, Conceptualization. **Yongle Lv:** Methodology, Investigation, Formal analysis, Conceptualization. **Fei Xie:** Investigation, Data curation. **Yanqiang Zhao:** Investigation. **Bowen Ren:** Investigation. **Shanshan Jin:** Supervision, Funding acquisition. **Ningxin Zhu:** Investigation. **Man Qin:** Supervision. **Zhiqiang Lin:** Supervision. **Lei Wang:** Supervision, Resources, Conceptualization. **Yuanyuan Wang:** Supervision, Resources, Funding acquisition.

Ethics approval

All animal experiments were conducted at Peking University Health Science Center, with the approval of the Institutional Animal Care and Use Committee (IACUC; PUIRB-LA2024107).

Declaration of competing interest

The authors declare that there is no conflict of interests.

Acknowledgments

This work was supported by the National Natural Science Foundation of China (No.82401083), the National Natural Science Foundation of China (No.82470944), the Beijing Natural Science Foundation (NO.7244445), and the China Postdoctoral Science Foundation (No. 2023M730117).

Appendix A. Supplementary data

Supplementary data to this article can be found online at https://doi.

org/10.1016/j.biomaterials.2026.123985.

Data availability

Data will be made available on request.

References

[1] AAE position statement on vital pulp therapy, J. Endod. 47 (9) (2021) 1340–1344.
[2] T.A. Wynn, A. Chawla, J.W. Pollard, Macrophage biology in development, homeostasis and disease, Nature 496 (7446) (2013) 445–455.
[3] Y.Z. Lu, et al., CGRP sensory neurons promote tissue healing via neutrophils and macrophages, Nature 628 (8008) (2024) 604–611.
[4] B.M. Sicari, et al., The promotion of a constructive macrophage phenotype by solubilized extracellular matrix, Biomaterials 35 (30) (2014) 8605–8612.
[5] M. Goldberg, et al., Inflammatory and immunological aspects of dental pulp repair, Pharmacol. Res. 58 (2) (2008) 137–147.
[6] S. Gordon, Alternative activation of macrophages, Nat. Rev. Immunol. 3 (1) (2003) 23–35.
[7] S. Gordon, F.O. Martinez, Alternative activation of macrophages: mechanism and functions, Immunity 32 (5) (2010) 593–604.
[8] H. Huang, et al., Development of rat caries-induced pulpitis model for vital pulp therapy, J. Dent. Res. 102 (5) (2023) 574–582.
[9] F.M. Lira Chavez, et al., Restoring the infected powerhouse: mitochondrial quality control in sepsis, Redox Biol. 68 (2023) 102968.
[10] L. Xu, et al., Macrophage polarization mediated by mitochondrial dysfunction induces adipose tissue inflammation in obesity, Int. J. Mol. Sci. 23 (16) (2022).
[11] J. Van den Bossche, et al., Mitochondrial dysfunction prevents repolarization of inflammatory macrophages, Cell Rep. 17 (3) (2016) 684–696.
[12] M. Giacomello, et al., The cell biology of mitochondrial membrane dynamics, Nat. Rev. Mol. Cell Biol. 21 (4) (2020) 204–224.
[13] L.C. Tábara, M. Segawa, J. Prudent, Molecular mechanisms of mitochondrial dynamics, Nat. Rev. Mol. Cell Biol. 26 (2) (2025) 123–146.
[14] L. Du, et al., IGF-2 preprograms maturing macrophages to acquire oxidative phosphorylation-dependent anti-inflammatory properties, Cell Metab. 29 (6) (2019) 1363–1375.e8.
[15] F. Xu, et al., Annexin A5 regulates hepatic macrophage polarization via directly targeting PKM2 and ameliorates NASH, Redox Biol. 36 (2020) 101634.
[16] Y. Zheng, et al., Macrophage polarization in rheumatoid arthritis: signaling pathways, metabolic reprogramming, and crosstalk with synovial fibroblasts, Front. Immunol. 15 (2024) 1394108.
[17] Y.L. Cao, et al., MFN1 structures reveal nucleotide-triggered dimerization critical for mitochondrial fusion, Nature 542 (7641) (2017) 372–376.
[18] Y.J. Li, et al., Structural insights of human mitofusin-2 into mitochondrial fusion and CMT2A onset, Nat. Commun. 10 (1) (2019) 4914.
[19] T. Koshiba, et al., Structural basis of mitochondrial tethering by mitofusin complexes, Science 305 (5685) (2004) 858–862.
[20] E. Zacharioudakis, et al., Modulating mitofusins to control mitochondrial function and signaling, Nat. Commun. 13 (1) (2022) 3775.
[21] A. Franco, et al., Correcting mitochondrial fusion by manipulating mitofusin conformations, Nature 540 (7631) (2016) 74–79.
[22] M. Li, et al., A ROS-responsive hydrogel incorporated with dental follicle stem cell-derived small extracellular vesicles promotes dental pulp repair by ameliorating oxidative stress, Bioact. Mater. 36 (2024) 524–540.
[23] Y. Zhao, et al., Injectable CNPs/DMP1-loaded self-assembly hydrogel regulating inflammation of dental pulp stem cells for dentin regeneration, Mater. Today Bio 24 (2024) 100907.
[24] S. Kanvah, et al., Oxidation of DNA: damage to nucleobases, Acc. Chem. Res. 43 (2) (2010) 280–287.
[25] B.D. Freudenthal, et al., Uncovering the polymerase-induced cytotoxicity of an oxidized nucleotide, Nature 517 (7536) (2015) 635–639.
[26] C. Luna-Marco, et al., Cardiovascular benefits of SGLT2 inhibitors and GLP-1 receptor agonists through effects on mitochondrial function and oxidative stress, Free Radic. Biol. Med. 213 (2024) 19–35.
[27] B. Mu, et al., Oxidative stress-mediated protein sulfenylation in human diseases: past, present, and future, Redox Biol. 76 (2024) 103332.
[28] T.O. Waheed, et al., Oxidative stress response in adipose tissue-derived mesenchymal stem/stromal cells, Int. J. Mol. Sci. 23 (21) (2022).
[29] L. Zhang, et al., Thermosensitive injectable in situ forming hydrogel incorporating anti-oxidative stress and anti-inflammatory nanoparticles for vital pulp therapy of pulpitis, Mater. Today Bio 31 (2025) 101482.
[30] Y. Lv, Y. Xu, S. Zhang, et al., Rapidly Photocurable and Strongly Adhesive Hydrogel-Based Sealant with Good Procoagulant Activity for Lethal Hemorrhage Control, Adv. Funct. Mater. 35 (40) (2025) 2501904.
[31] K. Zheng, et al., Flexible bicolorimetric polyacrylamide/chitosan hydrogels for smart real-time monitoring and promotion of wound healing, Adv. Funct. Mater. 31 (34) (2021) 2102599.
[32] S. Jana, S.K. Levengood, M. Zhang, Anisotropic materials for skeletal-muscle-tissue engineering, Adv Mater 28 (48) (2016) 10588–10612.
[33] P. Yu, et al., Mechanistically scoping cell-free and cell-dependent artificial scaffolds in rebuilding skeletal and dental hard tissues, Adv Mater 34 (46) (2022) e2107922.
[34] P. Dai, et al., A novel methacryloyl chitosan hydrogel microneedles patch with sustainable drug release property for effective treatment of psoriasis, Macromol. Biosci. 23 (12) (2023) e2300194.
[35] B. Li, et al., Hydrosoluble, UV-crosslinkable and injectable chitosan for patterned cell-laden microgel and rapid transdermal curing hydrogel in vivo, Acta Biomater. 22 (2015) 59–69.
[36] G. Li, et al., An injectable liposome-anchored teriparatide incorporated gallic acid-grafted gelatin hydrogel for osteoarthritis treatment, Nat. Commun. 14 (1) (2023) 3159.
[37] M. Shin, E. Park, H. Lee, Plant-inspired pyrogallol-containing functional materials, Adv. Funct. Mater. 29 (43) (2019).
[38] A.J. Valente, et al., A simple ImageJ macro tool for analyzing mitochondrial network morphology in mammalian cell culture, Acta Histochem. 119 (3) (2017) 315–326.
[39] D. Wang, et al., *Long non-coding RNA IGFBP7-AS1 accelerates the odontogenic differentiation of stem cells from human exfoliated deciduous teeth by regulating IGFBP7 expression*, Hum Cell 35 (6) (2022) 1697–1707.
[40] A. Nanchen, T. Fuhrer, U. Sauer, Determination of metabolic flux ratios from 13C-experiments and gas chromatography-mass spectrometry data: protocol and principles, Methods Mol. Biol. 358 (2007) 177–197.
[41] V.A. Portnoy, et al., Deletion of genes encoding cytochrome oxidases and quinol monooxygenase blocks the aerobic-anaerobic shift in Escherichia coli K-12 MG1655, Appl. Environ. Microbiol. 76 (19) (2010) 6529–6540.
[42] N. Zhu, et al., Silver-doped bioactive glass/chitosan hydrogel with potential application in dental pulp repair, ACS Biomater. Sci. Eng. 5 (9) (2019) 4624–4633.
[43] J. Van den Bossche, D.L. Saraber, Metabolic regulation of macrophages in tissues, Cell. Immunol. 330 (2018) 54–59.
[44] W.L.O. da Rosa, E. Piva, A.F. da Silva, Disclosing the physiology of pulp tissue for vital pulp therapy, Int. Endod. J. 51 (8) (2018) 829–846.
[45] S. Chen, et al., Macrophages in immunoregulation and therapeutics, Signal Transduct. Targeted Ther. 8 (1) (2023) 207.
[46] M. Allegra, Redox systems, oxidative stress, and antioxidant defences in health and disease, Antioxidants 10 (12) (2021).
[47] C. Tziafa, et al., Dentinogenic responses after direct pulp capping of miniature swine teeth with biodentine, J. Endod. 40 (12) (2014) 1967–1971.
[48] J. Tian, et al., Dental follicle stem cell-derived small extracellular vesicles ameliorate pulpitis by reprogramming macrophage metabolism, Bioact. Mater. 51 (2025) 179–196.
[49] Z. Xie, et al., Antimicrobial Peptide- and dentin matrix-functionalized hydrogel for vital pulp therapy via synergistic bacteriostasis, immunomodulation, and dentinogenesis, Adv. Healthcare Mater. 13 (18) (2024) e2303709.
[50] M. Wang, et al., Irisin-loaded cerium-containing mesoporous bioactive glass for effective immunomodulation and odontogenesis of dental pulp cells, Adv. Sci. (Weinh.) (2025) e01567.
[51] V. Piccolo, et al., Opposing macrophage polarization programs show extensive epigenomic and transcriptional cross-talk, Nat. Immunol. 18 (5) (2017) 530–540.
[52] M.J. Davis, et al., Macrophage M1/M2 polarization dynamically adapts to changes in cytokine microenvironments in Cryptococcus neoformans infection, mBio 4 (3) (2013).
[53] X.T. He, et al., Role of molybdenum in material immunomodulation and periodontal wound healing: targeting immunometabolism and mitochondrial function for macrophage modulation, Biomaterials 283 (2022) 121439.
[54] A.S. Rambold, E.L. Pearce, Mitochondrial dynamics at the interface of immune cell metabolism and function, Trends Immunol. 39 (1) (2018) 6–18.
[55] J.K. Dowling, et al., Mitochondrial arginase-2 is essential for IL-10 metabolic reprogramming of inflammatory macrophages, Nat. Commun. 12 (1) (2021) 1460.
[56] S.T. Decker, K. Funai, Mitochondrial membrane lipids in the regulation of bioenergetic flux, Cell Metab. 36 (9) (2024) 1963–1978.
[57] C.H. Yao, et al., Mitochondrial fusion supports increased oxidative phosphorylation during cell proliferation, eLife 8 (2019).
[58] K.S. Lee, X. Su, T. Huan, Metabolites are not genes - avoiding the misuse of pathway analysis in metabolomics, Nat. Metab. 7 (5) (2025) 858–861.
[59] T. Di, et al., ECM remodeling by PDGFRβ+ dental pulp stem cells drives angiogenesis and pulp regeneration via integrin signaling, Stem Cell Res. Ther. 16 (1) (2025) 283.
[60] Q. Feng, et al., Phillygenin improves diabetic nephropathy by inhibiting inflammation and apoptosis via regulating TLR4/MyD88/NF-κB and PI3K/AKT/GSK3β signaling pathways, Phytomedicine 136 (2025) 156314.
[61] J. Liu, et al., Exercise induced meteorin-like protects chondrocytes against inflammation and pyroptosis in osteoarthritis by inhibiting PI3K/Akt/NF-κB and NLRP3/caspase-1/GSDMD signaling, Biomed. Pharmacother. 158 (2023) 114118.
[62] C.C. Huang, et al., Exosomes as biomimetic tools for stem cell differentiation: applications in dental pulp tissue regeneration, Biomaterials 111 (2016) 103–115.
[63] M. Florimond, et al., Modulators of wnt signaling pathway implied in dentin pulp complex engineering: a literature review, Int. J. Mol. Sci. 23 (18) (2022).
[64] M. Li, et al., Histology-based profile of inflammatory mediators in experimentally induced pulpitis in a rat model: screening for possible biomarkers, Int. Endod. J. 54 (8) (2021) 1328–1341.
[65] L. Zhou, et al., Fusobacterium nucleatum exacerbates the progression of pulpitis by regulating the STING-dependent pathway, FASEB J. 38 (1) (2024) e23357.